2019-01-01

Interactions Of Bacterial Communities With Hydrous Sulfate Minerals In Water-Restricted Gypsic Environments: A Case Study Based In The White Sands National Monument

Brandon Nicholas Lajoie
University of Texas at El Paso

INTERACTIONS OF BACTERIAL COMMUNITIES WITH HYDROUS SULFATE MINERALS IN WATER-RESTRICTED GYPSIC ENVIRONMENTS: A CASE STUDY BASED IN THE WHITE SANDS NATIONAL MONUMENT

BRANDON NICHOLAS LAJOIE

Master's Program in Geological Sciences

APPROVED:

Jie Xu, Ph.D., Chair

Benjamin Brunner, Ph.D.

Anthony Darrouzet-Nardi, Ph.D.

Stephen Crites, Ph.D.
Dean of the Graduate School

Dedication

To everyone who impacted the completion of this work.

The UTEP Administrative and Technical Staff: Annette, Amber, Kirsten, Carlos, Michael Lyubchenko

The people who guided and advised me: Jie, Ben, Rip, and Anthony

My Lab Mates: Ezequiel, Matt, Muammar, and Hugo

My family and friends

And everyone else

INTERACTIONS OF BACTERIAL COMMUNITIES WITH HYDROUS SULFATE MINERALS IN WATER-RESTRICTED GYPSIC ENVIRONMENTS: A CASE STUDY BASED IN THE WHITE SANDS NATIONAL MONUMENT

by

BRANDON NICHOLAS LAJOIE, BS

THESIS

Presented to the Faculty of the Graduate School of

The University of Texas at El Paso

in Partial Fulfillment

of the Requirements

for the Degree of

MASTER OF SCIENCE

Department of Geological Sciences

THE UNIVERSITY OF TEXAS AT EL PASO

August 2019

Abstract

Microbial communities have been commonly found to survive and thrive in arid to hyper-arid gypsic environments that are considered hostile to most other forms of life. The mechanisms through which microbes have conquered these harsh environments remain poorly understood. Here I hypothesize that the microbial communities in water-restricted gypsic settings could benefit in terms of energy and water sources via their interactions with the abundant hydrous sulfate minerals [i.e., gypsum (CaSO4·2H2O)] that build up these niches. Gypsum is of high bio-relevance because its sulfate component may be used as electron acceptor by sulfate-reducing bacteria and the crystallization water may be released as untapped water source along with the bacterial scavenging of sulfate. The focus of this study is to investigate if sulfate-reducing bacteria are significant within the existing bacterial communities in water-limited gypsic environment and if the bacterial interaction with gypsum provides essential support for the overall bacterial communities. I based this study at the White Sands National Monument, which contains the largest field of gypsum sand dunes in the world, in association with deflation plains and evaporite flats and obtained samples at various locations and depths. By analyzing the various biogeochemical components of the collected samples, including indigenous bacterial nucleic acids, associated mineral compositions and morphology and field geochemical conditions, I aim to constrain the relationship between the abundance and composition of bacterial communities and the modification of hydrous sulfate minerals reflected in their compositional and morphological variations. The major tools I used include real-time PCR (qPCR), 16S amplicon sequencing, X-ray diffraction (XRD), and scanning electron microscopy (SEM). The sediments at various depths from the investigated five distinct sites are primarily composed of gypsum with considerable amounts of glauberite present in most samples. Basanite and anhydrite as well as calcite and dolomite were also identified in certain samples. Bacterial communities exist at readily recoverable levels in all collected sediments but higher overall abundances (up to 5 orders of magnitude higher) are associated with top layers of the sediments where there is the presence of water. Preliminary

results also showed that significant sulfate-reducing communities exist in the samples form Alkali Flat and inter-dune puddles only, where the highest amounts of 16S genes were recovered. The SEM analysis revealed higher heterogeneity in terms of the minerals' sizes and morphology in the crust samples compared to those at depth, indicative of higher extent of modification, either biologically or abiotically. Slimy aggregates that are comparable to biofilm structures were directly observed in some of the sediment crusts. The agreement between qPCR data of 16S and *dsrA* genes and coincidence of higher levels of those data with increased heterogeneity in sediment mineralogy lend credence to the hypothesis that the SRB may play a critical role mediating the habitability of water-restricted gypsic environments.

Table of Contents

Dedication iii

Abstract v

Table of Contents vii

List of Tables ix

List of Figures x

Background 1

- Gypsic Environments 1
- Sulfur Reducing Bacteria 3
- Motivation for this Work 4

Methodology 7

- Site Description 7
- Sample Acquisition 9
- DNA Extraction 10
- Real-Time (Quantitative) Polymerase Chain Reaction 10
- X-Ray Diffraction 12
- Scanning Electron Microscopy 13

Results 15

- Overall bacterial abundances – A depth- and site-specific pattern 15
- Mineralogy of bulk sediments – XRD analysis 15
- Detail variations in sediments' mineralogy and morphology – SEM analysis 17

Discussion 19

- Depth-dependent abundance of bacterial communities 19
- Bacterial Related Mineralogical Variations 19

Conclusions 22

- Bacterial Communities at Depth 22
- XRD at Depth 22
- SEM. 23

References.....47

Vita 54

List of Tables

Table 1: 24

List of Figures

Figure 1: 24
Figure 2a: 25
Figure 2b: 25
Figure 2c: 26
Figure 2d: 26
Figure 2e: 27
Figure 2f: 27
Figure 2g: 28
Figure 3: 29
Figure 4a: 30
Figure 4b: 30
Figure 4c: 31
Figure 4d: 31
Figure 4e: 32
Figure 5: 33
Figure 6S: 34
Figure 6a: 35
Figure 6b: 36
Figure 6c: 37
Figure 6d: 38
Figure 6e: 39
Figure 7a: 40
Figure 7b: 41
Figure 7c: 42
Figure 7d: 43
Figure 8: 44
Figure 9: 45
Figure 10: 46

Background

GYPSIC ENVIRONMENTS

Gypsic environments are classified by the presence of gypsum ($CaSO_4 \cdot 2H_2O$), the most common sulfate mineral on Earth, as one of the dominant minerals. These environments are often extremely hostile to life due to limited water availability. Gypsum can form as either a primary mineral, in any environment where evaporation outpaces water input such as hypersaline lakes, marine-marginal sabkhas, gypsiferous soils, gypsum dune fields, coastal lagoons, and salt crusts, or as a secondary mineral near hydrothermal vents due to interactions of sulfide oxidizing bacteria and local emissions (Shahid et al., 2007, Natalicchio et al., 2014, Farias et al, 2017, Takai et al., 2008, Glamojica et al., 2012, Barbieri and Stivaletta et al., 2011). Gypsic deposits are commonly associated both with a history of water loss, and with modern aridity, which due to the relatively high solubility of gypsum can allow for the motion of gypsum into permeable layers often further restricting water availability. This intense lack of water is the key feature that limits life within gypsic environments.

These environments are widespread and can be found in a variety of depositional makeups within most of the arid zones that cover roughly 28% of the Earth's surface (Hughes and Lawley 2003; Barbieri and Stivaletta 2011; N. Stivaletta et al. 2012; McKay et al 2016). Some notable examples of gypsic environments include La Brava, a hypersaline lake located in the Salar de Atacama of Chile (Farias et al, 2017), Abu Dhabi, a location within the United Arab Emirates with vast gypsic sabkha (Shahid et al., 2007) and globally widespread gypsiferous soils (Poch et al., 1998). La Brava lies within a restricted basin that receives very little precipitation. The water that is received is acquired from groundwater that passes through the gypsum concentrated rock underneath the lake. This low amount of water input coupled with the shift of humidity with

seasons causes the lake to cycle between gaining stages, when humidity is relatively high and inputs from groundwater exceed evaporation, and falling stages, when dissolved sediments crystallize out of solution due to the increased evaporation of water. The Abu Dabi gypsic sabkha is formed by humidity from the coast allowing for rainfall in an otherwise record setting hot, arid area. Precipitation interacts with the soil to cause mobility of minerals upward as precipitated water hits an impermeable surface at a depth that still allows for evaporation from the soil causing minerals dissolved from the previous impermeable base to rise incrementally through the trapped water. Gypsiferous soils such as those found in Catalonia, Spain highly affect the ability of plants to grow due to the difficulty of removing water from these soils. This is due to the gypsum lowering water availability to plants by making it harder to take in by the removal of pore space, otherwise allowing for continued growth or water transport, within the soil by gypsum crystallization (Poch et al., 1998).

Despite the water restriction of gypsic environments, microorganisms have commonly been found living within, to the point of near exclusivity. Gypsum is of high bio-relevance because its sulfate component is likely bioavailable as an electron acceptor for sulfate-reducing bacteria, an important group of microorganisms in both geological and ecological contexts. Some places already identified with thriving communities of these microorganisms include the Atacama Desert, Chile, the Mojave Desert, United States, perennial springs in Nunavut, Canada, the acid brine lakes of Western Australia, rock coatings in Lappland, Sweden, and the Al-Jafr Basin, Jordan (Stivaletta et al., 2011, Glamojica et al., 2012, Zentilli et al., 2019, Benison and Bowen, 2013, Marnocha and Dixon, 2014, Dong et al., 2007). These bacteria have shown several adaptations that allow them to better survive in gypsic environments such as preference of crystal type and texture (Dong et al., 2007), communal strategies against high salt, irradiation, and heavy metal conditions in more

halite dominated environments (Stivaletta et al., 2011), close association with communities of photosynthetic microbes that regulate the nitrogen cycle at (Glamoclija et al. 2012), and the use of gypsum as a physical barrier against UV radiation, freeze–thaw cycles, and desiccation (Wierzchos et al. 2015).

SULFUR REDUCING BACTERIA

Sulfate reducing bacteria (SRB) have been important organisms through much of Earth's 4.6-billion-year history (Shen and Buick, 2004). Isotopic evidence indicates that sulfate reduction evolved at least 3.7 billion years ago, well before the evolution of oxygenic photosynthesis and cyanobacteria (Shen et al., 2001). Sulfate reducing bacteria utilize sulfate as electron acceptors and drive half of the sulfur cycle by transforming sulfate into sulfide. By coupleing to sulfate reduction, SRB can utilize various substrates as electron donors, the most common ones include hydrogen and reduced carbon. In numerous previous studies, SRB were found to be major contributors to endolithic microbial mats identified in a wide range of natural settings (Baumgartner et al., 2006, Visscher et al. 1992), including some of the extreme gypsic environments (Hughes and Lawley 2003).

Sulfate reducing bacteria are also of relevance for environmental remediation and resource recovery processes. For example, SRB have been evaluated extensively for their potential in immobilizing metals released into aquatic environments via different processes (e.g., acid mine drainage, nuclear test contaminations, and anthropogenic release). The use of SRB may result in direct (enzymatic) or indirect (non-enzymatic) reduction of certain metal(loid) anions, such as U, Cr, Mo, and Se, leading to the formation of less soluble products realizing the sequestration. For metal cations, the reduction of sulfate to sulfide by SRB induces precipitation of dissolved metals as metal sulfides that generally have exceedingly low solubilities. Bioremediation involving SRB

has been demonstrated to be effective for a variety of metal(loid)s including U, Cr, Mo, Se, Cd, Co, Cu, Fe, Ni, and Zn. Due to SRB's tolerance to a wide range of pH and saline conditions, they will continue to receive substantial attention in the bioremediation of natural habitats and scenarios (Neculita et al., 2007, Muyzer and Stams, 2008). Based on the same principles of immobilizing metal(loid), SRB are also used to enrich and recover precious resources. One example of this is their utility in removing toxins from gold ores, making the process cost effective. In this instance bacteria can be added to the system to change the toxins, such as arsenic, to a non-bioavailable or immobile form by changing its oxidation state (Gumulya et al., 2018, Valls and Lorenzo, 2002). Research of SRB is also carried out in the oil industry, especially in the production process, as they are often naturally found in reservoirs and cause production of hydrogen sulfide gas, which is toxic and speeds corrosion of pipelines and equipment. In these cases, the research is mainly related to the extermination of SRB or the removal of hydrogen sulfide produced by SRB (Tang et al., 2008).

Previous laboratory studies have showed that SRB can capitalize on solid-phase sulfate minerals including gypsum (Karnachuk et al., 2002). This utilization is dependent on sulfate being freed and taken into the cell before it can be reduced. This is achieved by the SRB causing dissolution and precipitation reactions to take place so as to access the sulfate otherwise stuck in the crystal. It remains elusive, however, if the SRB-sulfate mineral (i.e., gypsum) interactions are extensive in natural scenarios or play a key role in supporting the overall associated microbial communities.

MOTIVATION FOR THIS WORK

Microbial communities have commonly been found to survive in hyper arid gypsic environments that are hostile to most other forms of life. The reasons for this are poorly understood

and are hypothesized to involve interactions between the various microorganisms in the associated bio-communities and the minerals of the surrounding landscape. Despite this, microorganisms have been identified living in many of these gypsic settings obviously using strategies not available to other kinds of life and that previous studies have started to investigate. What remains unknown however is if it is possible for these bacterial communities to utilize the gypsum around them as both a source of energy, as is the case of sulfur reducing bacteria (SRB) populations which can use sulfate as an electron acceptor, and a source of water due to the amount trapped within the crystal structure of gypsum. Examples of potential reactions used by these bacteria for the reduction of sulfate to sulfide can be seen in **Equation 1** (M. Mansor et al. 2019) **and 2** (J. Westrich and R. Berner, 1984) using different organic carbons as electron donors.

$$2\ C_2H_4OHCOO^- + SO_4^{2-} \rightarrow 2\ CH_3COO^- + 2\ HCO_3^- + HS^- + H^+ \quad \textbf{(Eqn. 1)}$$

$$2\ CH_2O + SO_4^{2-} \rightarrow H_2S + 2HCO_3^- \quad \textbf{(Eqn. 2)}$$

Understanding how bacterial communities may alter hydrate sulfate minerals (i.e., gypsum) will particularly advance our current understanding of bacterial survival mechanisms, especially those dependent on associated mineral environments under water-restricted conditions. In the terrestrial realm, the potential water source obtained from microbial decomposition/transformation of gypsum would greatly modify our overall view of the biosphere-geosphere relationship, specifically on how the biosphere may influence the habitability of the geosphere. The process used by the SRB, if proven to effectively free water from the crystal structure of gypsum, may also allow for utilization of previously untapped water resources in regions where gypsum is present, both on Earth and in extraterrestrials (i.e., Mars).

The focus of this study is on bacteria-sulfate mineral interactions in water-restricted gypsic environments, particularly to constrain if there is a relationship between the overall abundance and

composition of bacterial communities, and the modification extent of the matrix minerals (i.e., gypsum) that can be used to predict the habitability of gypsic settings. The location of White Sands National Monument, NM was selected due to its high gypsum content and the bacterial communities previously identified there (Glamoclija et al, 2012).

Methodology

Site Description

The White Sands National Monument, located near Alamogordo, NM, is one of the largest gypsum dune fields in the world. The area is comprised almost entirely of gypsum and gypsic minerals. This is because runoff from the Pleistocene glaciers, containing soluble minerals such as gypsum, from the San Andreas and Sacramento Mountains entered the restricted Tularosa basin and formed Lake Otero which later dried leaving behind the gypsic minerals in the modern playa Lake Lucero and Alkali Flats. These deposited minerals were subject to wind erosion throughout the Holocene and formed the present-day dunes (NPS, 2019). Sample acquisition began with scouting out locations of interest around White Sands National Monument and during scouting five distinct sites within the monument were identified and sampled. All the sites as seen in **Figure 1** have distinct properties within the monument and several photos of the sites can be seen in **Figure 2**. Playa Lake Site is located in a small playa lake on the eastern margin of the dune field. The playa covers approximately 1.5 acres or 0.6 hectares. When dry the playa has a light yellowish-brown surface and is set approximately 1 m below the undulating, heavily vegetated sand sheet that surrounds it. The playa has a generally flat, but rough surface due to salt crystal growth and desiccation. There is a gentle slope that rises from the floor of the playa to the scarp that marks the eroded edge of the playa. The samples were collected from the playa surface, approximately 3 m from the edge of the slope. The playa sediments are generally young. The vegetated sand sheet in which the playa formed after the emplacement and stabilization of the white sands dune field. The dune field dates to between 7,200 years ago and 5,800 years, as dated by OSL underlying lake sediments and in foredune and dammed stream deposits that postdate dune field formation (Fryberger, 2001; Langford et al., 2003, 2009, Kocurek et al., 2007). Stabilization of the dune field is estimated from preserved hearths on stabilized dunes, that all post-date 4,200 BP. (Blair, Clark,

& Wells, 1990). Worman et al. (2018) suggested that the front of the dune field had advanced ruing the late Holocene and that the present-day front of the dune field, associated with the playa lake, dates to the Pueblo period, dating between 1,000 to 1,400 AD. This would make the playa younger than 1,000 years old. The processes active in the playa require a balance of wind erosion of the dry playa surface, which creates the depression in which the playa sits, and wind deposition of dust, precipitation of gypsum in and on the surface, and erosion of the playa margin, that fill the eroded playa. When water tables are persistently low, the playa is excavated, and when water tables are higher, new sediment is deposited in the floor of the playa. Therefore, the sediments within the playa are probably much younger than 1,000 years and probably date to post 2,000's, 1950's, 1930's droughts. The sediment at site one is probably essentially a modern feature.

Interdune Site is located in an interdune near the western edge of the barchan area and the eastern edge of the main dune ridge (see Fryberger, 2003 or Kocurek et al., 2007 for location of these features). The interdune is approximately 120 by 450 m, and is elongate NW-SE, perpendicular to the dune slip faces and migration directions. The site was selected in a barren topographic low on the interdune, near the downwind margin. The site exposed evaporite polygons, however 2 m to the north and east, rugose erosional ridges left by a migrating dune are evident. The surface was only exposed after passage of the dune, and therefore, the surface has only been near to the surface for less than 10 years. The sediment themselves are probably older. Kocurek et al., 2007 though OSL dated the lake muds below the aeolian sand to 7,200 ybp. Langford et al. (2003, 2009) estimated the modern main dune ridge to within the last 1,000 years. And this is probably the maximum probable age of these sediments.

Alkali Flat Site is a modern saline playa along the western margin of the Alkali Flat. The site is frequently flooded and is filling a depression excavated by the wind approximately 1,000

years ago. The playa is elongate north-to-south, and is 1.3 km wide and approximately 20 km long, Sediments in the playa are soft, and euhedral crystals of salt precipitated in the saline muds, they are almost certainly historical, recent deposits. Unique to Site 3 was also the lowered pH of the groundwater, tested by pH strip to be around 5 and a noticeably darker sediment.

Interdune Puddle Site and Near Interdune Puddle Site are near each other along the western margin of the dune field. They are found in low-lying, frequently flooded areas where fresh-water outflow from water that infiltrated the dune field seeps near the surface (Newton and Allen, 2014). The age constraints on the deposits are similar to those at Interdune Site. However, the surface has been exposed for at least 80 years, longer than at site 2 (McKee, 1966). Interdune Puddle Site comprised of several standing pools of water caused by recent precipitation. Near Interdune Puddle Site was a dry area containing several crusts proximal to Interdune Puddle Site and was taken for comparison to the saturated site.

SAMPLE ACQUISITION

All sampling for this project's purposes took place during November, 2018 which is considered to be part of the dry season, despite the recent precipitation. The sampling began by removing a representative identified surface crust in the vicinity of the selected site. Depth profile samples were collected by auguring into the sediment with an ice augur and removing scrapings from the wall of the borehole at regular intervals with a metal spatula until the water table was reached. The augur and metal spatula used to gather these samples were sanitized with 75% ethanol and wiped down before and after each use to avoid contamination. Gathered samples were stored in sealed autoclaved plastic containers and kept in a cooler with dry ice to preserve them. Upon return to the university all samples were stored in a -80ºC freezer until used. Prior to further analyses the collected samples were divided in a UV-sterilized laminar hood into two subsamples,

one for the extraction of nucleic acid contents and the other for X-ray diffraction and Scanning Electron Microscope sediment analysis.

DNA EXTRACTION

The DNA extraction was done with a DNeasy PowerSoil Extraction Kit inside a clean hood. Procedure on the kit was followed with tared ~0.25g amounts of sample. An extraction blank was run containing no sample alongside every extraction in order to better detect contamination. Samples were run through a Thermo Scientific NanoDrop One Spectrophotometer after extraction for an estimate of DNA content and purity. The DNA was then diluted to lessen the effects of any inhibitors contained within the raw extraction with DNA free water to a uniform value per extraction run. Due to the dilution being based on the spectrophotometer data that suffered from accuracy issues at low concentrations all DNA concentrations at this step were approximate and this data was only used to determine how much dilution of each sample for inhibitors was possible. Several rounds of extractions were required for enough material for later study and as such each extraction varied in biological and sediment content slightly. Slight variances in mass were also unavoidable and data derived from extractions is normalized to the mass of sediment used in the extraction process in order to limit the effects of mass differences.

REAL-TIME (QUANTITATIVE) POLYMERASE CHAIN REACTION

The qPCR process utilizes a gene specific primer with florescence probes which binds to certain segments of DNA. The DNA is separated into single strands during the denaturing process which allows for the primer to attach to the specified gene if present. After the primer attaches to the gene of interest during the annealing process the gene is replicated during the extension process, doubling the amount of DNA containing the selected gene, before a signal is registered and then the process starts again with the newly copied DNA also being denatured. This is repeated

for several cycles while the fluorescent probes attached to the primers give off signal during the extension process taking place between each cycle. Each cycle is expected to double the amount of gene of interest present. The time it takes for the signal to reach a threshold intensity is then recorded by the device as cycle time (Ct). Comparing the Ct values of different samples allows for calculations of concentrations prior to the PCR process and thus comparisons of concentrations of the selected genes in tested samples. In this study extracted DNA was analyzed to identify the abundance of 16S RNA gene, a universal gene in all bacteria, and *dsrA,* a marker gene in sulfate reduction pathways. In order to have a uniform standard for both 16S RNA and *dsrA* a strain of *Desulfovibrio Vulgaris* was used for the concentration curve for both tests. One tube of Mastermix was created for each qPCR run immediately before hand by combining 10µL of SYBR Green, 3µL of DNA free water, and 2µL of either the 16S or the *dsrA* primers per PCR well. Aliquots of this mix were then put in separate microcentrifuge tubes and 5µL of sample DNA, previously diluted to a uniform concentration, per PCR well was added. After samples were mixed and briefly centrifuged to ensure total inclusion of all added materials the PCR prepped DNA was added to PCR wells and briefly centrifuged to ensure no bubbling of the solution. All samples were prepared and run in triplicate as to assure quality. The samples were then loaded into an Analytikjena qTower^3 Real-Time PCR Thermocycler and the template for the PCR run was designed using Analytikjena's qPCRsoft 3.2. Depending on which primer was used the temperature conditions for the run were set to be optimal. The 16S primer set consisted of forward primer 5'-GGA GGC AGC AGT RRG GAA T-3 and reverse primer 5'-GAC GGG CGG TGT GTR CAA-3' with lengths of 347-365 and 1390-1409 base pairs respectively and had melt temperatures of 62 and 64.7 degrees Celsius respectively. For the 16S primer set the sample was brought to 98ºC for 2.5 minutes before beginning the cycling process. One cycle consisted of being held at 95ºC for 30 seconds, being

held at 58ºC for 1 minute, and finally being held at 72ºC for 1.5 minutes and scanned. These cycles were repeated thirty-five times before a melting curve from 60-90ºC was generated to ensure sample consistency. The *dsrA* primer, designed in previous studies (Kondo et al. 2004), was brought to 95ºC for 15 minutes before beginning the cycling process. One cycle consisted of being held at 95ºC for 15 seconds, held at 60ºC for 30 seconds, and being held at 72ºC for 30 seconds before being scanned. Forty cycles were run after which a melting curve from 65-95ºC was generated to ensure consistency. In order to compare between runs data was normalized to concentrations instead of the slightly variable Ct values. The concentration values were calculated by comparing the unknown samples to a sample of D. Vulgaris diluted to 1 ng/µL, 100 pg/µL, 10 pg/µL, and 1 pg/µL run through the PCR process alongside the unknowns. A conversion between Ct and concentration was then made using the 4 standards as the basis of a curve. From these concentrations and primers, the number of base pairs per gram of sediment was then calculated.

X-RAY DIFFRACTION

XRD allows for characterization of the crystal phases present in a sample by exposing it to an X-ray beam and detecting the diffraction angles of the deflected beam. The angle that the X-ray beam is deflected at after hitting the sample is dependent on the crystal/atomic structure of the minerals interacting with the beam. The process gives a distinctive set of peaks that can be compared to known mineral spectra to identify the various minerals and crystal habits present in a sample. Samples were stored in an incubator at 45ºC for 24 hours to remove free water and then ground with a mortar and pestle to a fine powder to make all crystal sizes uniform. After this the samples were affixed onto a glass slide with amber paste and scanned using a Rigaku MiniFlexII desktop X-ray diffractometer. The scan range was from 2Θ 10-60 at a speed of 0.5 degrees per second. The software JADE was used to export all data into Excel and to locate peaks. Reference

peaks for expected and potentially present minerals were acquired from American Mineralogist Crystal Structure Database and were used as references to identify minerals present in sediment samples. Reference and Sample peaks were then compared using Microsoft Excel and Powerpoint. Due to slight variations in both glass slide, paste, and sample thickness minor adjustments were required for sample comparison. The gypsum peak at 11.64 2Θ was selected as the corrective point as it was both isolated from any other expected peaks and the smallest 2Θ value of significant intensity.

SCANNING ELECTRON MICROSCOPY

Scanning Electron Microscopy utilizes a beam of electrons that is scanned over the sample. This beam interacting with the materials present will then give a variety of signals which are processed to form an image of the material in question. These images can reach a scale of μm making it useful for identifying features and processes on the micro and nano scale. The back-scattering beam of this model also allows distinguishing between materials based on their electron density with more dense materials appearing as brighter on the images. The same materials prepped for XRD were also used in SEM. Materials were left in an incubator at 45ºC for 24 hours and then were adhered to double sided carbon tape before being further affixed to a stand. This stand was inserted into a chamber within the Hitachi TM-1000 SEM and a vacuum state was achieved before the scanning process started. Scanning Electron Microscopy utilizes a beam of electrons that scans the sample. The interaction between beam and scanned materials produces signals which allow to produce a high-resolution image of the scanned surface. Such images can reach a scale of μm making it useful for identifying features and processes on the micro and nano scale. The back-scatteed beam also allows distinguishing between materials based on their electron density, with more dense materials appearing brighter on the images. The same materials prepped

for XRD were also used in SEM. Materials were left in an incubator at 45ºC for 24 hours and then adhered with double sided carbon tape to a stand. This stand was inserted into a vacuum chamber within a Hitachi TM-1000 SEM. Several images of Playa Lake Site and Alkali Flat Site were produced at all sampled depths to changes in bulk sediment and sample morphology at high resolution between two distinct sites at similar conditions. Additionally, images of samples from the dry sites' (i.e., Playa Lake, Interdune, Alkali Flats, and Near Interdune Puddle) surface crusts were collected to identify any changes in crust morphology that could indicate different community behavior between sites.

Results

OVERALL BACTERIAL ABUNDANCES – A DEPTH- AND SITE-SPECIFIC PATTERN

The bacterial populations vary based on location and depth and a comparison of all sites can be seen in **Figure 3** while individual sites with value tables can be found in **Figure 4**. The copy numbers for the recovered 16S rRNA genes from the various depths at different sites range from ~ 5×10^2 to 1.7×10^8 per gram of sediment. The Alkali Flats and Interdune Puddle Sites showed the highest abundance of 16S genes with the Near Interdune Puddle Site also having relatively high readings. I also recovered significant amounts of *dsrA* gene from these samples that contained the highest 16S genes (data shown in **Figure 5**). Relatively little *dsrA* genes were recovered from other sites. Sites Playa Lake and Interdune showed significantly less 16S signal and almost no *dsrA* gene copies with exception at Site Playa Lake 22cm depth. All DNA concentrations decreased with depth. The rate of decrease was not consistent between sites. Concentrations were also highly variable between different extractions of sediments from the same bulk sample. This is most prevalent in highly populated samples and less populated samples show less of a range.

MINERALOGY OF BULK SEDIMENTS – XRD ANALYSIS

All analyzed sediment samples, shared a basic mineralogical setup which was dominated by gypsum (**Figure 6**). The surface sample from Site Playa Lake has prominent gypsum peaks and several strong glauberite peaks, especially around 45º 2Θ. Sparse peaks corresponding to quartz, dolomite, and calcite are also present. At 12cm depth Site Playa Lake begins to show more glauberite peaks and stronger peaks for quartz, and dolomite. The calcite peak seems to be absent at this depth and there is a potential sulfur peak within a peak shoulder around 23º 2Θ. This suggests that, relative to the surface, this particular depth contains less gypsum. At 22cm depth Site Playa Lake now only displays the powerful gypsum peaks that have been present since surface, even more intense glauberite peaks, and two dolomite peaks. At 32cm depth Site Playa Lake keeps

its large gypsum peaks. The glauberite peaks diminish slightly and small anhydrite peaks are also present. There is a large increase in quartz in this sample with a major peak around 26º 2Θ. At 42cm depth the accessory peaks to gypsum may include glauberite, bassanite, sulfur, and dolomite. Due to the overlapping positions of the major peak for native sulfur with those of gypsum, we cannot confirm the presence or absence of it in the samples however. All accessory peaks seem to have diminished in intensity compared to 22cm depth. At the surface of Site Interdune gypsum is the dominant signature. The principle peak for bassanite is present and peaks for calcite, dolomite, quartz, and glauberite are present but the fractions are small. At 20cm depth there is a substantial increase in the amount of glauberite peaks. Quartz and bassanite peaks are slightly reduced with the main quartz peak being absent entirely. Dolomite and calcite amounts remain similar to surface levels. At 40cm there is another large increase of the signal of glauberite peaks. Bassanite and dolomite peaks have decreased while calcite has disappeared. There is a large decrease in the gypsum peak around 29º 2Θ. At 60cm depth the signal appears to collect more noise. Quartz now has the dominant peak though it is still much less proportionally than gypsum. The gypsum peak around 12º 2Θ is now diminished and displays a shoulder. Slight glauberite signal can be detected and it is much diminished from 40cm. Dolomite and calcite peaks become prominent around 37º 2Θ. Trace peaks of bassanite and sulfur are present. The surface of Site Alkali Flat is dominated by gypsum peaks and all other peaks are barely detected. Glauberite, calcite and dolomite are all present though barely detectable. Shoulder signal around 23º 2Θ may be sulfur signal though it is a slight ridge on the main peak that makes this suspect. At 10cm depth Site Alkali Flat has a loss of signal from several major gypsum peaks. The gypsum peak around 31º 2Θ is now dominant. Glauberite is detected on several peaks. Anhydrite, quartz, dolomite, and calcite may be present, although the signals for all of these minerals are quite weak. At 18.5cm depth the gypsum peaks

stay similar to 10cm depth. There is a massive increase in the amount of bassanite signal and an increase to dolomite as well. Glauberite and calcite stay relatively consistent compared to 10cm depth. At Site Interdune Puddle pools 1 and 2 are extremely similar. Both show a rather muted signal compared to other sites. All gypsum peaks aside from around 12º and 44º 2Θ are extremely diminished. Slight signals of bassanite and dolomite are present in both pools. Pool 3 has gypsum peaks similar to the other sites and overall a more distinct signal. Dolomite, anhydrite, glauberite, and quartz signals are present. Spot 1 of Site Near Interdune Puddle is gypsum dominated with slight glauberite signal. Bassanite dolomite and quartz all have signals as well. Spot 2 is nearly identical with the addition of a very faint calcite signal. Spot 2 at depth begins to show more prominent gypsum peaks at all points. Signals for all other minerals stay similar to surficial samples. Throughout all the scanned sites aragonite was able to be detected with a preference for depth though the signal was always quite weak. Halite was detected at the water tables of the Interdune and Alkali Flat sites and at 1-2cm depth of Site Near Interdune Puddle. Pyrite peaks were detected at all sites and depths except for Site Interdune with no discernable trend. What aligns with the principle peak of pyrite is quite small in all samples in comparison to other major peaks, though this may be due to overlapping signals.

DETAIL VARIATIONS IN SEDIMENTS' MINERALOGY AND MORPHOLOGY – SEM ANALYSIS

SEM images from all sites show a larger population of an unidentified prismatic to acicular mineral in instances with higher biologic abundance. This mineral, while not being able to be positively identified by the methods used, varies in size from a few nanometers to several micrometers in length. The mineral is brighter than surrounding sediment in the SEM images which suggests that it has a higher electron density and thus is likely to be a different material. Images of all site surfaces and Site 1 at depth can be seen in **Figure 7-10**. In addition to the presence

of the crystals in the surface crusts there appears to be an association between the location of the crystals and morphologies typical for biologic material, with crystals being both more abundant and larger when within a close proximity to organic matter. Biologic materials formed several biologic structures. These include strands that connect sediment grains, filaments that wrap in and around sediment grains, and coatings on and around recesses in the surrounding sediments. Such structures are found at all sites but there is a rapid drop in abundance with increasing distance from surface. The filaments and strands don't appear to be extant below the surface level in any of the sites sampled. The coating structure seems to be located near pits located within the sediment grains. Grains from deeper samples show fewer pits than their surficial counterparts.

Discussion

Depth-dependent abundance of bacterial communities

All sites showed a general trend of decreased biologic activity overall with increased depth, which may suggest that the community as a whole is dependent on phototrophs or on organic matter that is more refractory with depth. The rate of change in biologic abundance is largely dependent on the total abundance of the community with less abundant communities, such as Sites Playa Lake and Interdune, having a more linear decrease and higher abundance communities, such as Site Alkali Flat, having a logarithmic falloff. This further suggests that large bacterial communities are limited to near surface by some means unconstrained by this study. SEM images seem to confirm this as biologic structures detected at all site surfaces are rarely if at all present in deeper areas. Site Interdune Puddle was the second most abundant and all samples here were from surficial pools. This could indicate that instead of gypsum utilization freeing water for the bacterial community simply presence of large amounts of water ensure colony health and that sulfate mineral metabolization is insignificant in comparison.

Bacterial Related Mineralogical Variations

Of the areas sampled those that had a larger abundance of indicators for bacterial life showed an increased XRD signal of possible byproducts of sulfur cycling such as glauberite, pyrite, and bassanite as well as small quantities of dolomite and calcite. The coinciding presence of carbonate minerals and markers for bacteria suggest that the carbonates are either beneficial to or produced by the bacterial life, though the possibility of little to no interaction cannot be ruled out. Carbonate minerals form by several processes, including the generation of inorganic carbon by the microbes in presence of free calcium or magnesium that can be derived from metabolization of gypsum or minerals like epsomite, ($MgSO4{\cdot}7H2O$). The latter mineral has been identified in

White Sands by previous studies (Steven Ramirez, 2017). Preferentially colonizing near carbonate bearing gypsum sediments could be advantageous because carbonates act as buffers, counteracting high or low pH, which may interfere with the bacteria's life functions. Unfortunately, the answer to the question if presence carbonates are the cause or result of microbial presence cannot be answered in the framework of this particular study.

The unknown crystals detected by SEM have morphological similarities to glauberite (K.M.Bisson et al. 2015, B. Buck et al. 2011) and bassanite (T. Rabizadeh et al. 2014). However without additional information (for example EDS spectra) positive identification is not possible. Of the instances of biologic materials, the collections of "slimes" and "strands" match fairly well with previous studies SEM images of biofilms (Ikuma et al., 2013) and bacterial filaments (J. Cook et al., 2015) with filaments varying greatly in size and form. Since the SEM images show that crystals and presumed biologic materials are in proximity to each other it can be speculated that the various organisms that live within the crusts are either involved in the formation or degradation of the crystals. Based on changes in size and number of crystals and the high variability between acicular, bladed, and prismatic crystal habits it appears that fluxuating environmental conditions may impact the crystals resulting in holes and other defects. It is unknown whether this is a result of sulfur cycling as has been hypothesized, or if the different habits of the crystals have any impact on habitability. The pitting seen within the sediments at the surface is likely due to bacterial leeching as it is associated with biofilms and is not present at deeper intervals. If water were the primary driver of this pitting it should not only be present at the surface where sediment and precipitation can interact but also near the water table which was typically located at the bottom of the drilled holes. This leads to the conclusion that it is more likely that the bacteria are directly using the mineral, as postulated, in previous studies (Karnachuk et al., 2002). This, and the

potential presence of glauberite, pyrite, and bassanite corroborates our hypothesis that there is a significant a causal relationship between thriving bacterial communities in gypsic environments and the production of dehydrated sulfate minerals.

Conclusions

Bacterial Communities at Depth

Depth appears to be an important factor in community health and high bacterial abundances are largely restricted to the very near surface. This is interpreted as a dependence on the abilities of phototrophic microorganisms, although the exact reason for the dependence is not constrained in this study. The sites with high water tables had the highest abundances of 16S had much higher water tables and abundances rapidly drop with increased depth. These sites also had higher amounts of the *dsrA* gene present which indicates that there is a positive relationship between *dsrA* and 16S abundance. The specific microorganisms that make up these communities have yet to be constrained and further information in that regard may illuminate why there is such a rapid drop in abundance with depth. Investigations into other forms of life commonly found within communities, such as archaea, fungi, and plants may give more insight to how the community as a whole operates.

XRD at Depth

While gypsum is dominant in all samples and at all depths the amount and intensity of important secondary minerals does change. Glauberite and bassanite seem to have higher signals near to but not at the surface. Calcite, dolomite, aragonite and quartz may influence the habitability of the sediment. Since these minerals have prominent signal only at depth a direct relation relationship between microbial habitats and minerals cannot be established. Since no steps were taken to remove biologic material before the XRD scans it is possible that if there is a close relationship between biologic structures and glauberite or bassanite these biofilms may obstruct detection. Pyrite is also lost in the signals of more populous minerals. In the future an attempt at removal of gypsum or biologic components and quantification of secondary and trace minerals may allow for greater insight into this relationship.

SEM

SEM imaging has shown that surface crust samples contain a number of biologic structures that have a relationship with both the distinct crystals seen in the images and the scours on the sediment grains. These biologic structures include biofilms and filaments in a few different forms. The crystals associated with the biologic structures are also highly variable showing acicular, prismatic, and bladed habits depending on the exact site. Additionally, small defects and holes can be seen in several of the crystals. The identity of the crystals remains unknown but the material seems to have a higher electron density than the surrounding gypsum. The pitting associated with the presence of biofilms ceases to exist at depth which helps rule out the idea that it is caused by water dissolution from precipitation and the water table. This may suggest that the pitting is from bacterial leaching and would support the hypothesis that SRB utilizing gypsum improves the health of the local community as a whole.

Table 1: GPS Location of Sampling Sites in NAD84

Site	Latitude	Longitude
Playa Lake	32.79692	-106.212
Interdune	32.81743	-106.273
Alkali Flat	32.82603	-106.447
Interdune Puddle	32.80958	-106.312
Near Interdune Puddle	32.80508	-106.315

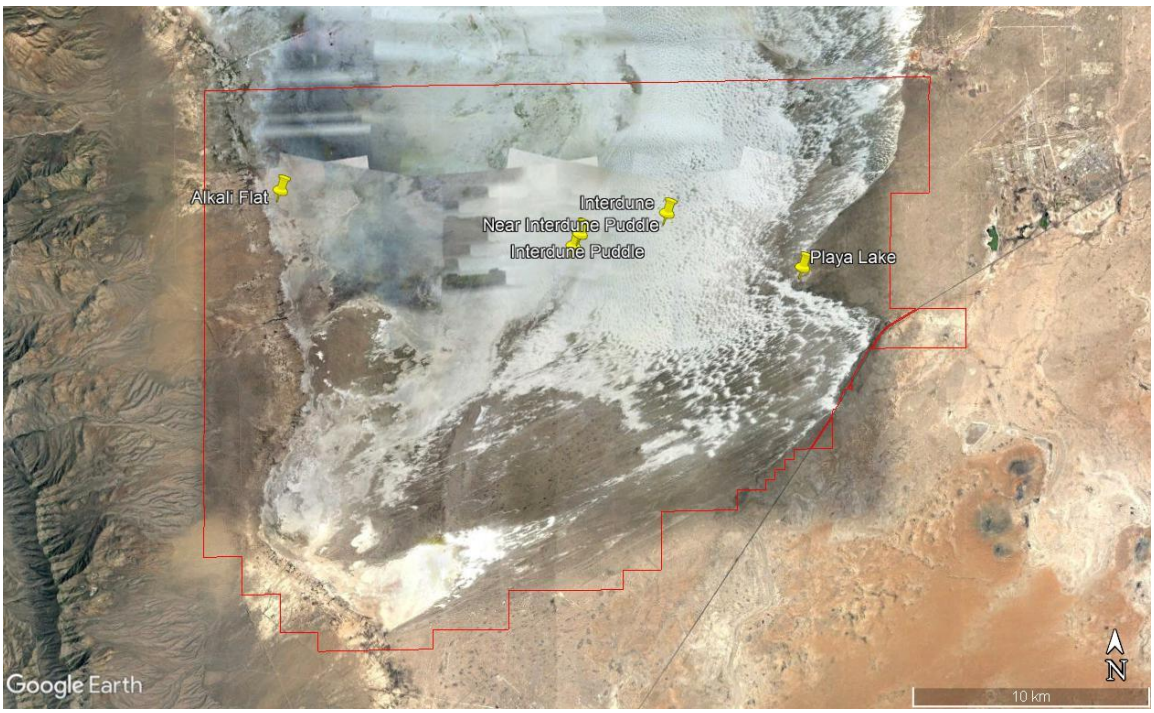

Figure 1: A map showing the areas sampled within the White Sands National Monument. The red line marks the border of the monument and the yellow pins represent the sampling sites. GPS locations of the sites can be found in Table 1.

Figure 2a: An image of sampling Site Playa Lake. Located at the center of a playa lake in the east of the park boundaries. (The copyright of the photo belongs to B. Brunner.)

Figure 2b: An image of the Site Playa Lake sediment at various depths. At each site surface crust was first sampled, and then we augured down to the water table and sampled at different depths. (The copyright of the photo belongs to B. Brunner.)

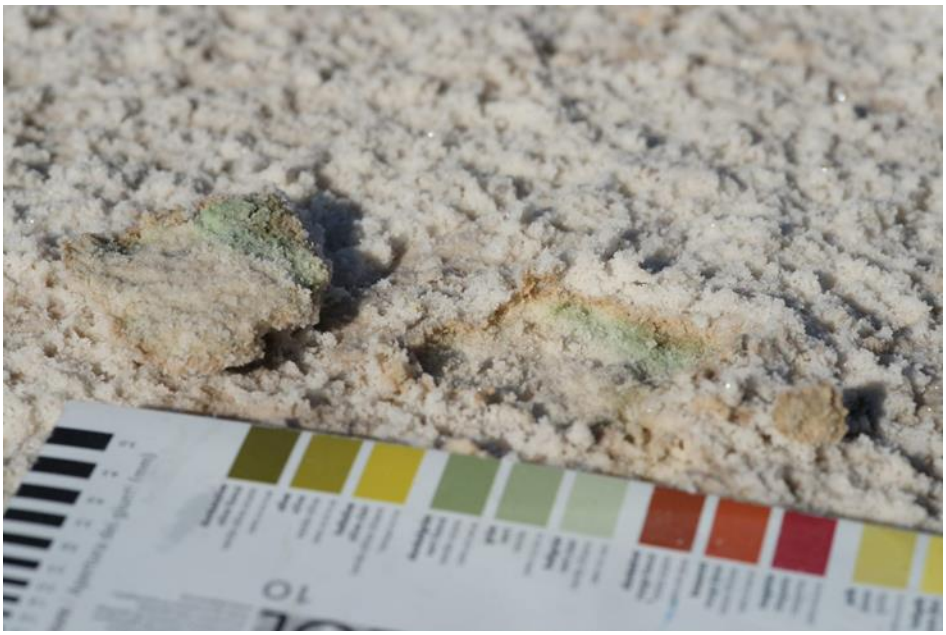

Figure 2c: A surface crust sample collected at Site Playa Lake. The bands have been interpreted as different dominant microbial communities in previous studies carried out at WSNM. (The copyright of the photo belongs to B. Brunner.)

Figure 2d: An image of Site Interdune. Located within an interdune section of the park. The augur used to create the holes can be seen in the ground. (The copyright of the photo belongs to B. Brunner.)

Figure 2e: An image of Site Alkali Flat. In this image, the shift in the sediment color can be seen by the material removed from the hole. (The copyright of the photo belongs to N. Cowgill)

Figure 2f: An image of the standing water at Site Interdune Puddle. (The copyright of the photo belongs to J. Xu.)

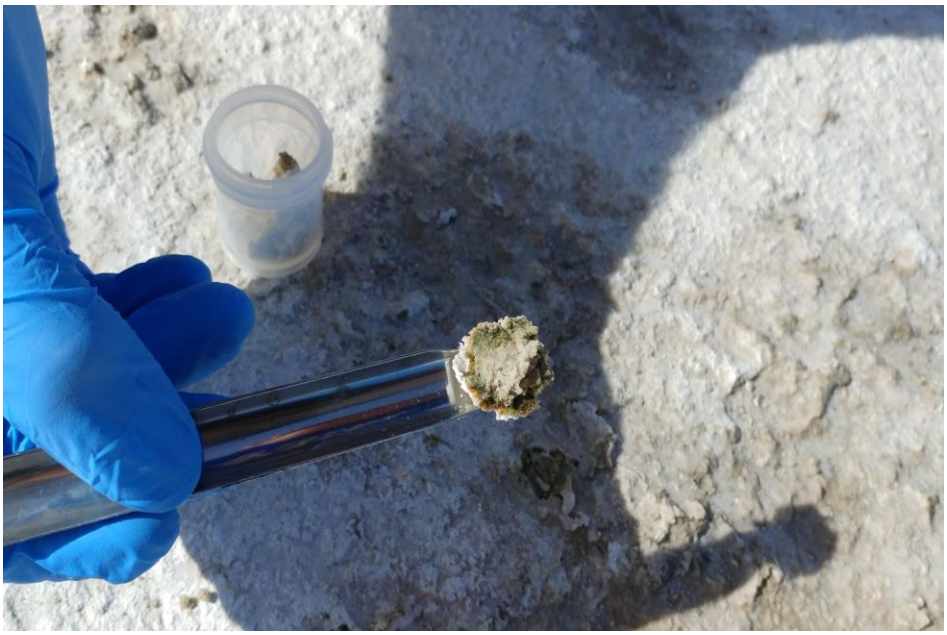

Figure 2g: An example of a surface crust sample collected at Site Near Interdune Puddle. (The copyright of the photo belongs to J. Xu.)

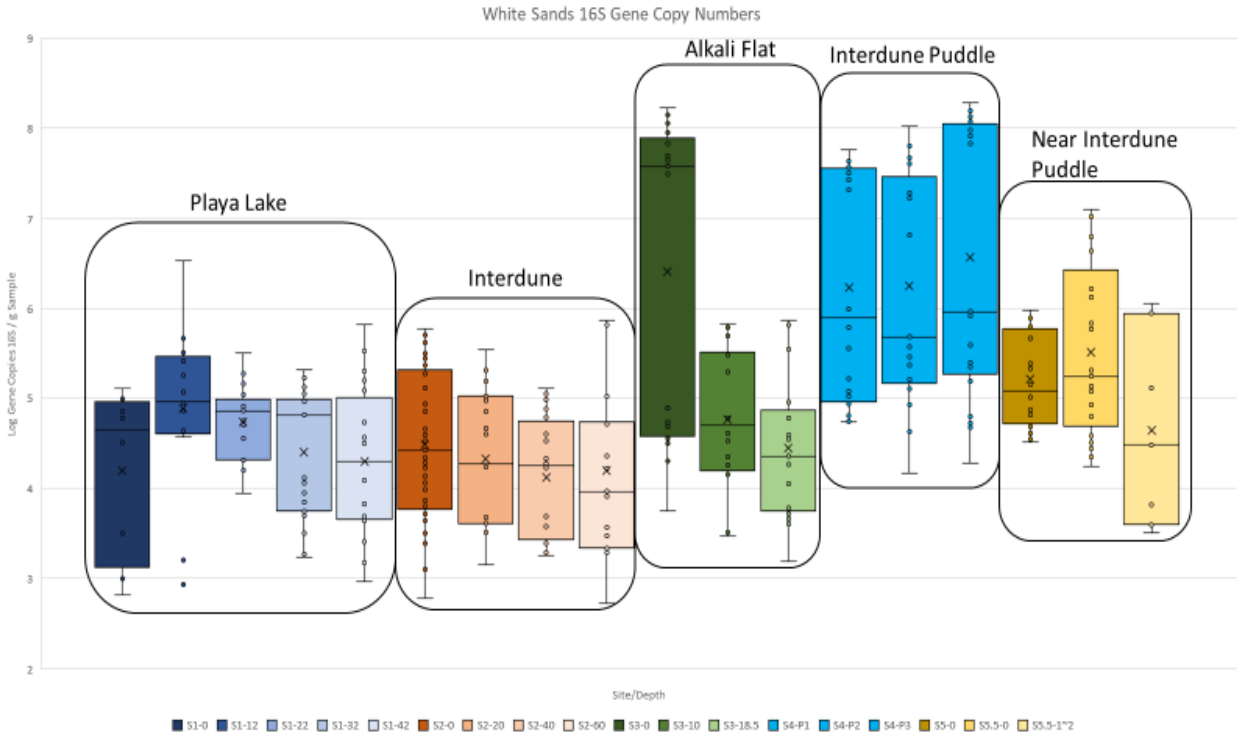

Figure 3: A comparative figure showing the copy numbers (in logarithm format) of 16S rRNA genes per gram of sediment. Samples at various depths from the same site are grouped by color. All collected data is displayed with the mean marked with an X, the median marked by the center bar, and the 25th and 75th quartile marks as the bottom and top of the boxes respectively. The whiskers of the plot show the extent of the data excluding outliers. Individual data points are marked with a circle.

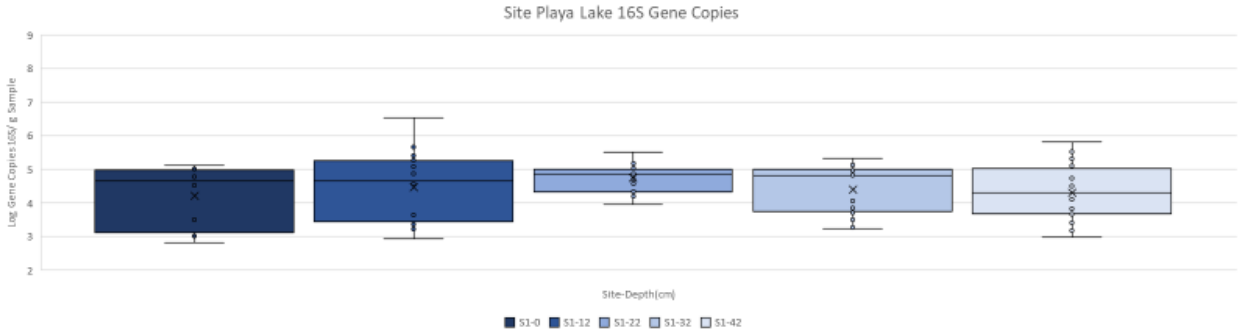

Name	S1-0	S1-12	S1-22	S1-32	S1-42
Upper Extreme	5.11	6.52	5.50	5.32	5.82
Upper Quartile	4.96	5.25	4.99	4.99	5.01
Median	4.65	4.64	4.86	4.82	4.30
Mean	4.20	4.46	4.74	4.40	4.30
Lower Quartile	3.12	3.44	4.32	3.75	3.66
Lower Extreme	2.81	2.94	3.95	3.24	2.97

Figure 4a: Details of the obtained 16S rRNA gene copy numbers per gram of sediment for Site 1 samples

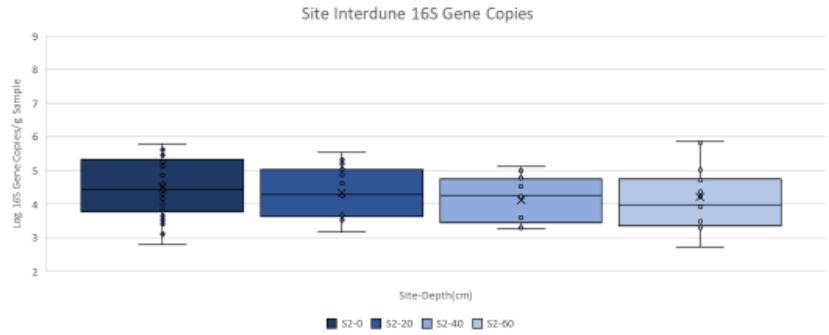

Name	S2-0	S2-20	S2-40	S2-60
Upper Extreme	5.78	5.54	5.11	5.86
Upper Quartile	5.32	5.03	4.75	4.74
Median	4.43	4.27	4.25	3.97
Mean	4.49	4.33	4.12	4.20
Lower Quartile	3.77	3.61	3.44	3.34
Lower Extreme	2.78	3.16	3.25	2.72

Figure 4b: Details of the obtained 16S rRNA gene copy numbers per gram of sediment for Site 2 samples

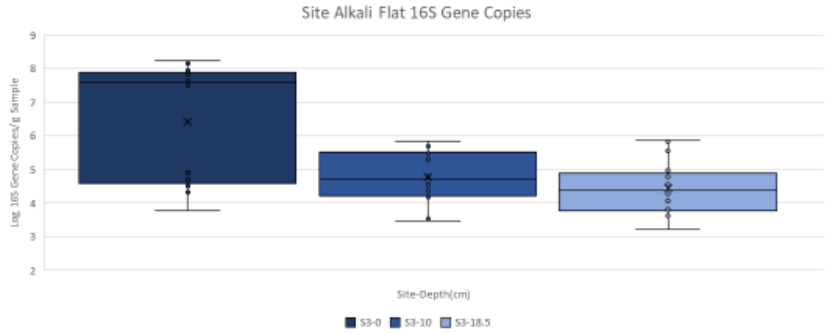

Name	S3-0	S3-10	S3-18.5
Upper Extreme	8.23	5.83	5.87
Upper Quartile	7.89	5.51	4.87
Median	7.58	4.70	4.36
Mean	6.41	4.77	4.45
Lower Quartile	4.58	4.20	3.75
Lower Extreme	3.75	3.47	3.20

Figure 4c: Details of the obtained 16S rRNA gene copy numbers per gram of sediment for Site 3 samples

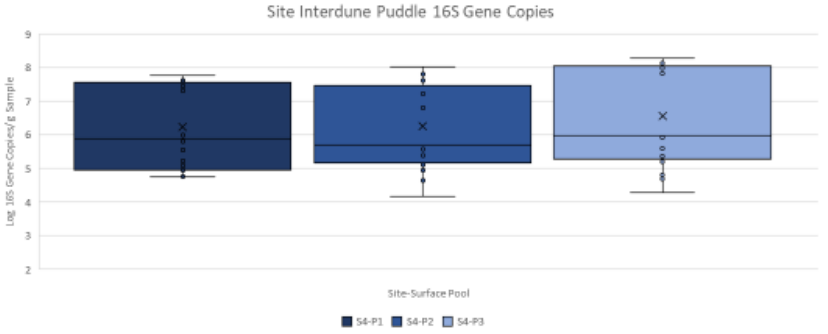

Name	S4-P1	S4-P2	S4-P3
Upper Extreme	7.76	8.02	8.28
Upper Quartile	7.55	7.46	8.05
Median	5.89	5.68	5.96
Mean	6.23	6.25	6.56
Lower Quartile	4.96	5.17	5.27
Lower Extreme	4.74	4.17	4.28

Figure 4d: Details of the obtained 16S rRNA gene copy numbers per gram of sediment for Site 4 samples

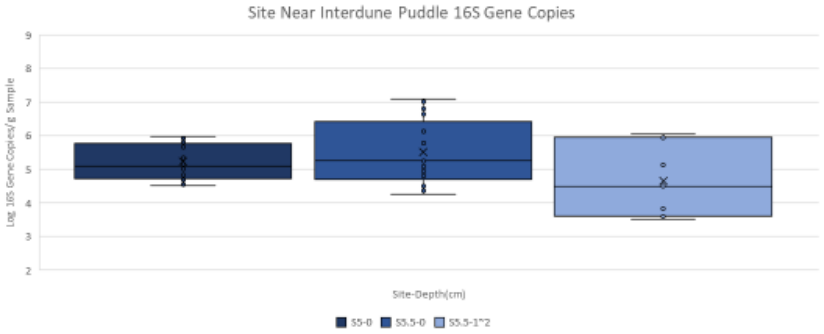

Name	S5-0	S5.5-0	S5.5-1~2
Upper Extreme	5.98	7.09	6.05
Upper Quartile	5.77	6.43	5.94
Median	5.09	5.25	4.49
Mean	5.22	5.51	4.65
Lower Quartile	4.72	4.69	3.60
Lower Extreme	4.52	4.25	3.51

Figure 4e: Details of the obtained 16S rRNA gene copy numbers per gram of sediment for Site 5 samples

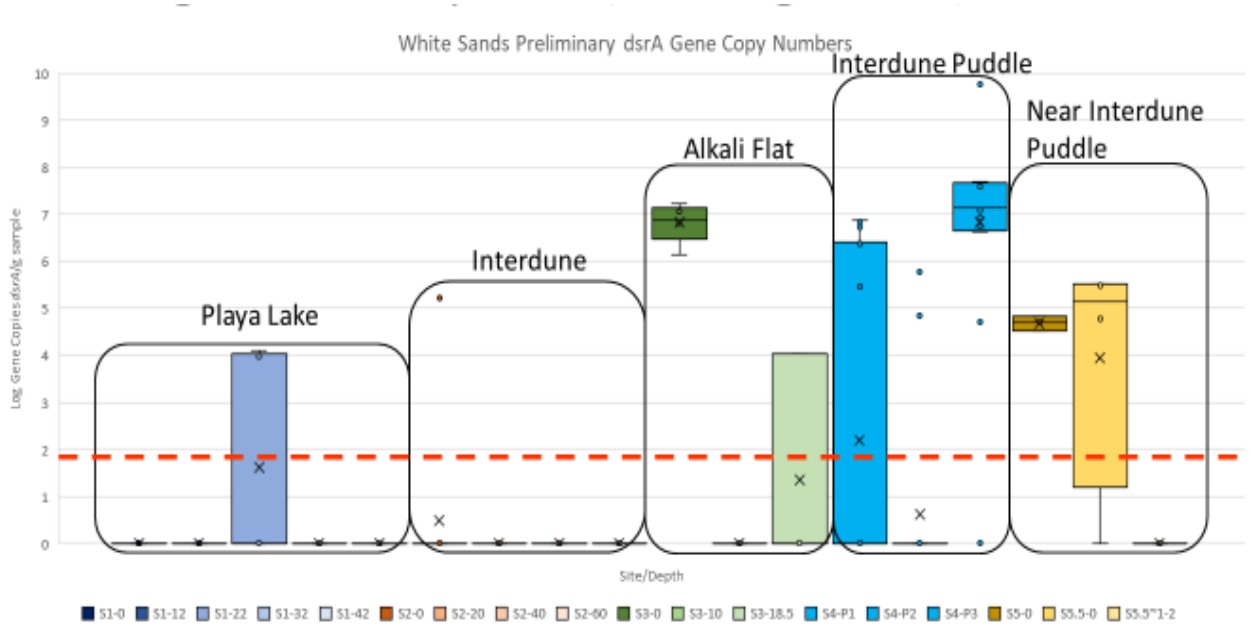

Figure 5: A comparative figure showing preliminary data of the copy numbers (in logarithm format) of *dsrA* genes per gram of sediment. Samples at various depths from the same site are grouped by color. All collected data is displayed with the mean marked with an X, the median marked by the center bar, and the 25th and 75th quartile marks as the bottom and top of the boxes respectively. The whiskers of the plot show the extent of the data excluding outliers. Individual data points are marked with a circle. Data under the orange line is considered unusable.

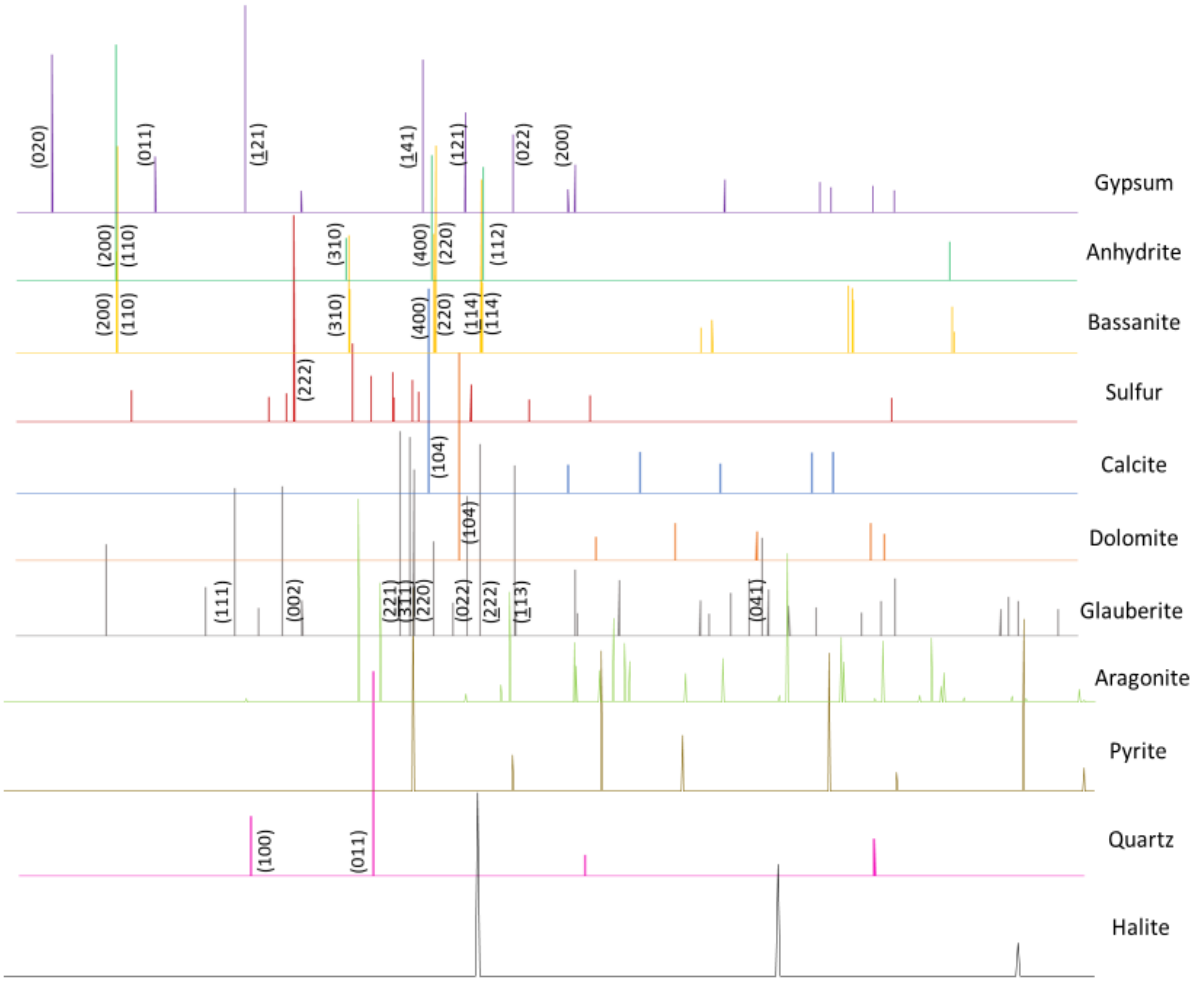

Figure 6S: Reference XRD spectra for major "gauge" minerals, some of which have been identified in the sediment samples. The displayed 2Θ range is from 10°-60°

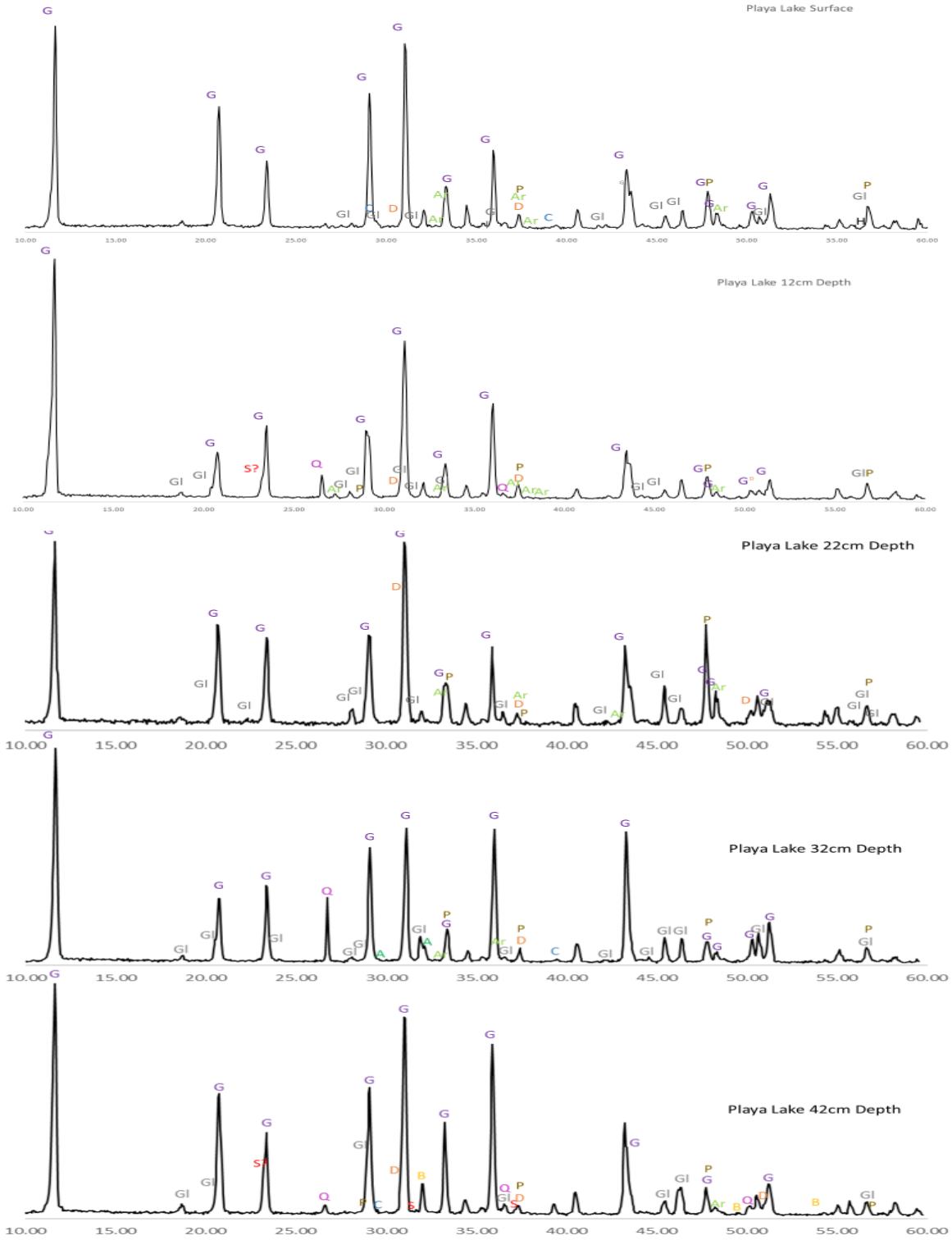

Figure 6a: Major mineralogical composition identified for the bulk sediment collected at various depths of Site Playa Lake. G-gypsum, Gl-glauberite, C-calcite, D-dolomite, A-anhydrite, P-pyrite, Ar- aragonite, H- halite and B-bassanite.

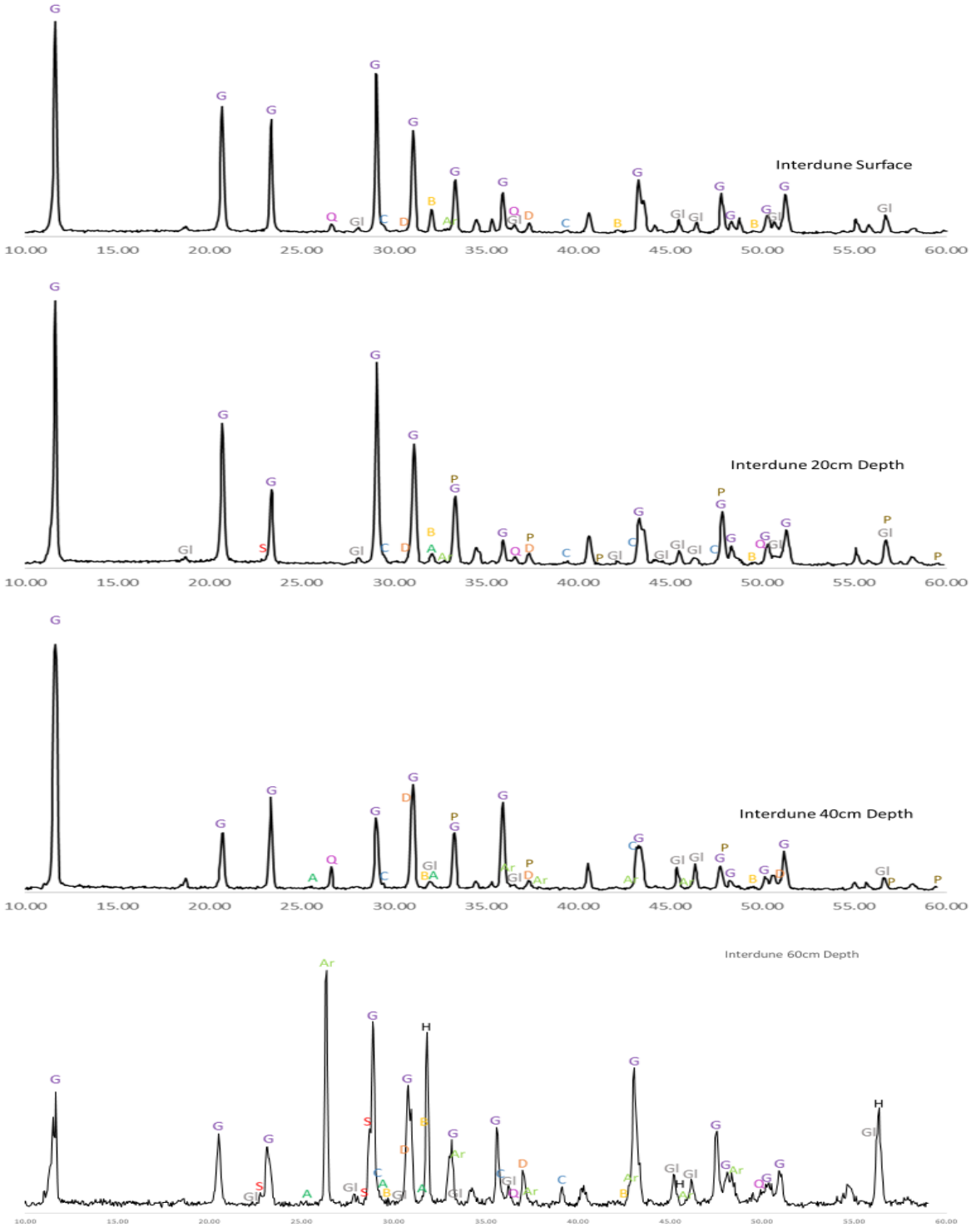

Figure 6b: Major mineralogical composition identified for the bulk sediment collected at various depths of Site Interdune. G-gypsum, Gl-glauberite, C-calcite, D-dolomite, A-anhydrite, P-pyrite, Ar- aragonite, H- halite and B-bassanite.

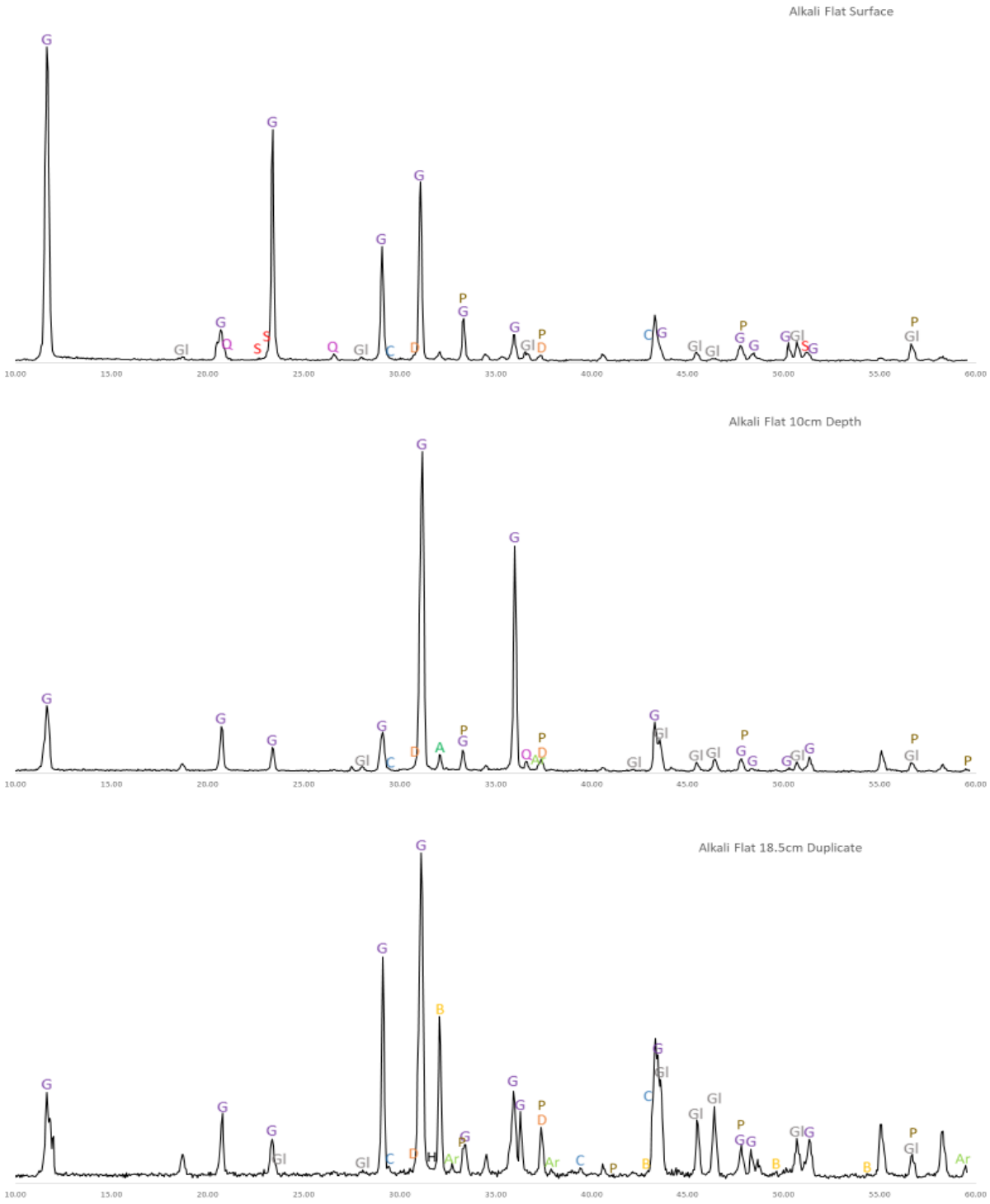

Figure 6c: Major mineralogical composition identified for the bulk sediment collected at various depths of Site Alkali Flat. G-gypsum, Gl-glauberite, C-calcite, D-dolomite, A-anhydrite, P-pyrite, Ar- aragonite, H- halite and B-bassanite.

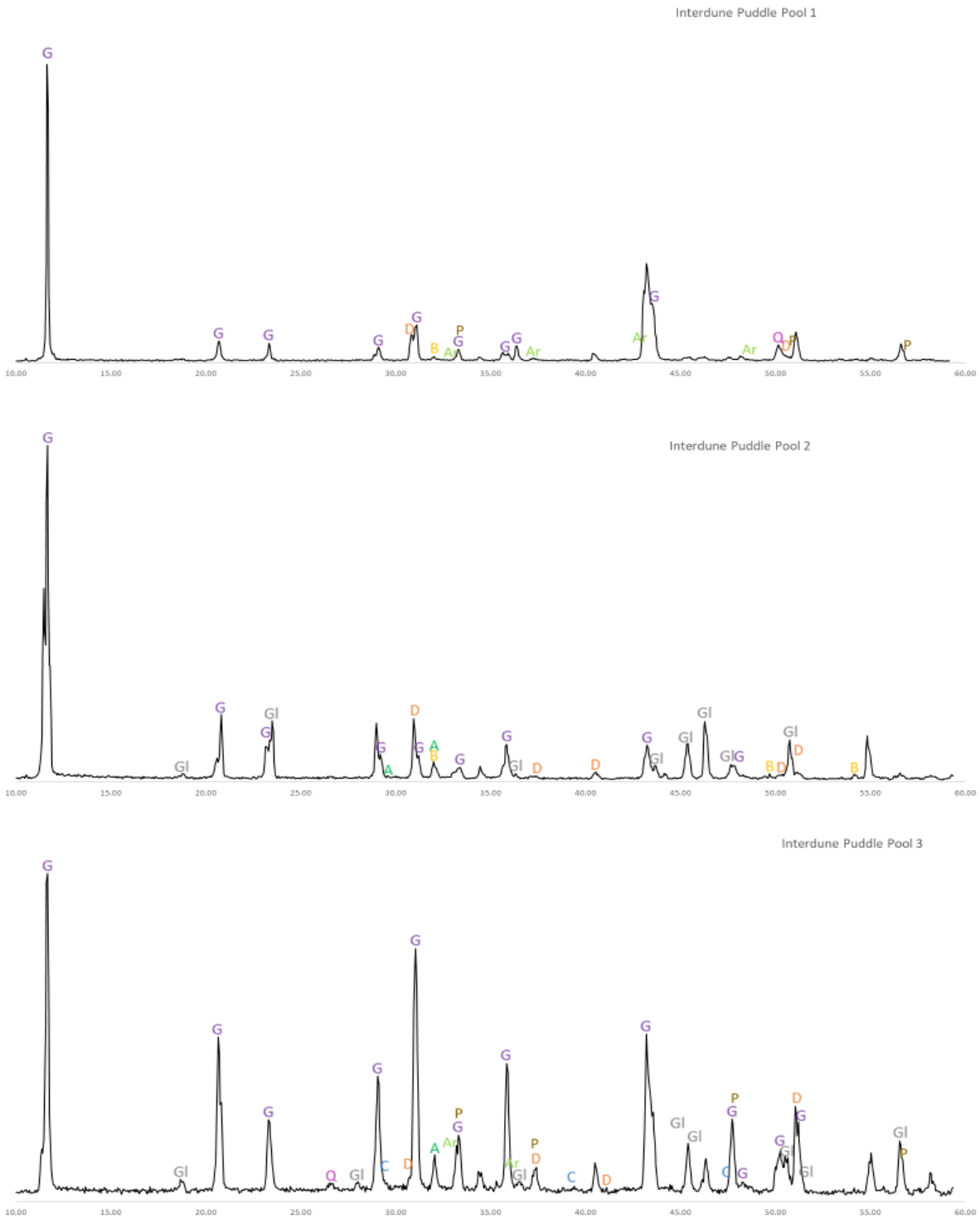

Figure 6d: Major mineralogical composition identified for the bulk sediment collected at various depths of Site Interdune Puddle. G-gypsum, Gl-glauberite, C-calcite, D-dolomite, A-anhydrite, P-pyrite, Ar- aragonite, H- halite and B-bassanite.

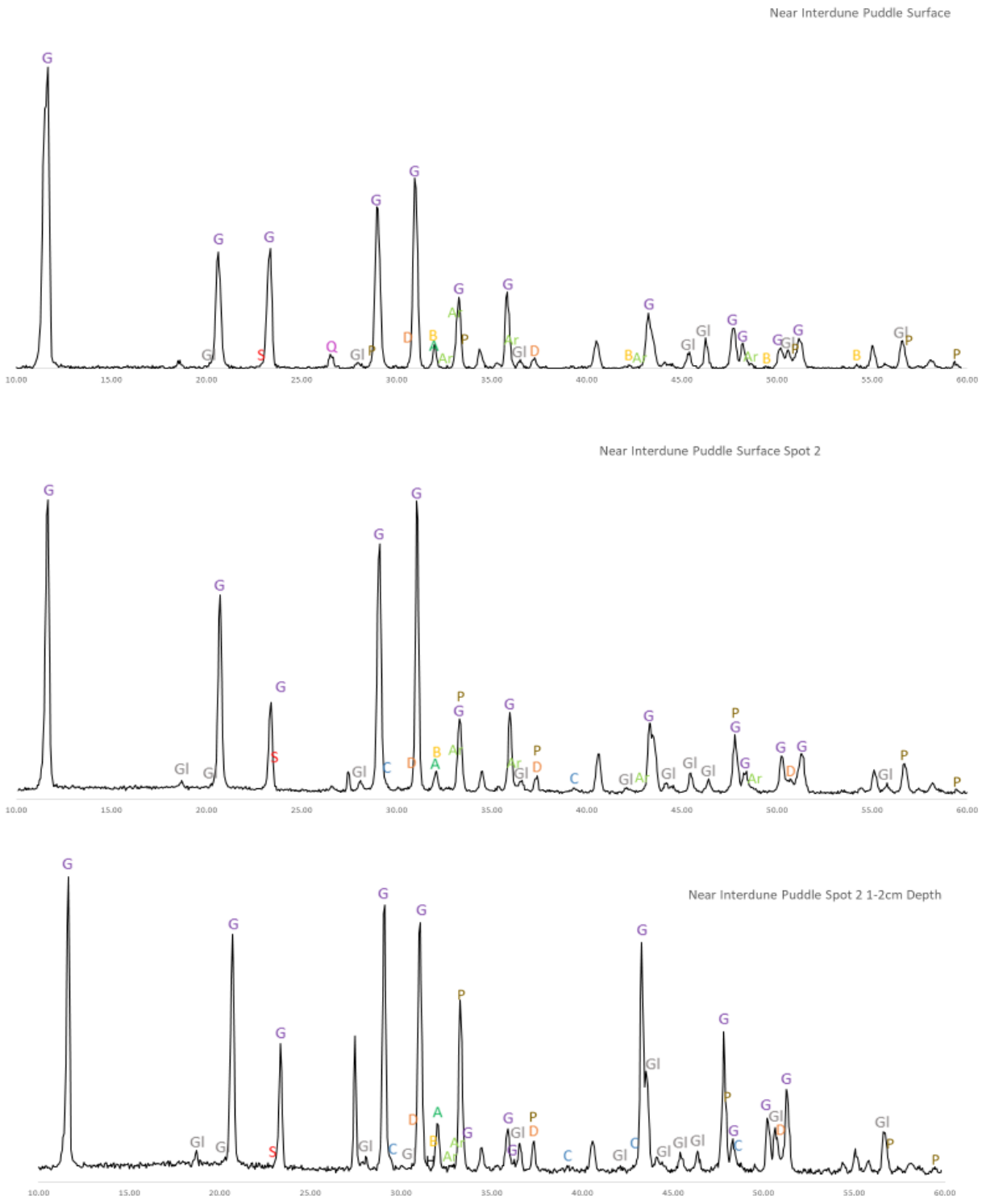

Figure 6e: Major mineralogical composition identified for the bulk sediment collected at various depths of Site Near Interdune Puddle. G-gypsum, Gl-glauberite, C-calcite, D-dolomite, A-anhydrite, P-pyrite, Ar- aragonite, H- halite and B-bassanite.

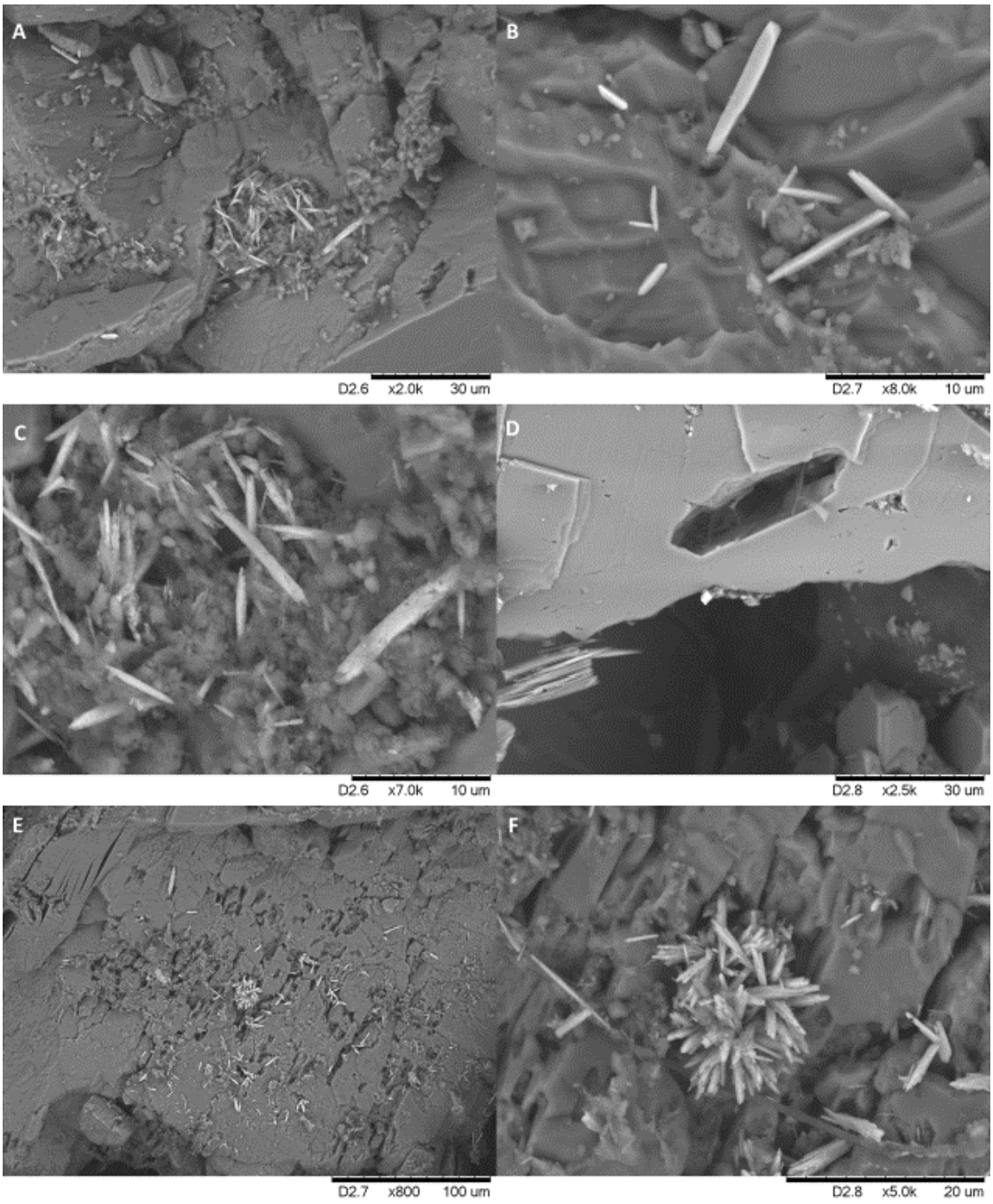

Figure 7a: Scanning electron micrographs of crust sediment samples from Site Playa Lake. Acicular crystals were identified. Pits and holes were also observed at the matrix grains' surface.

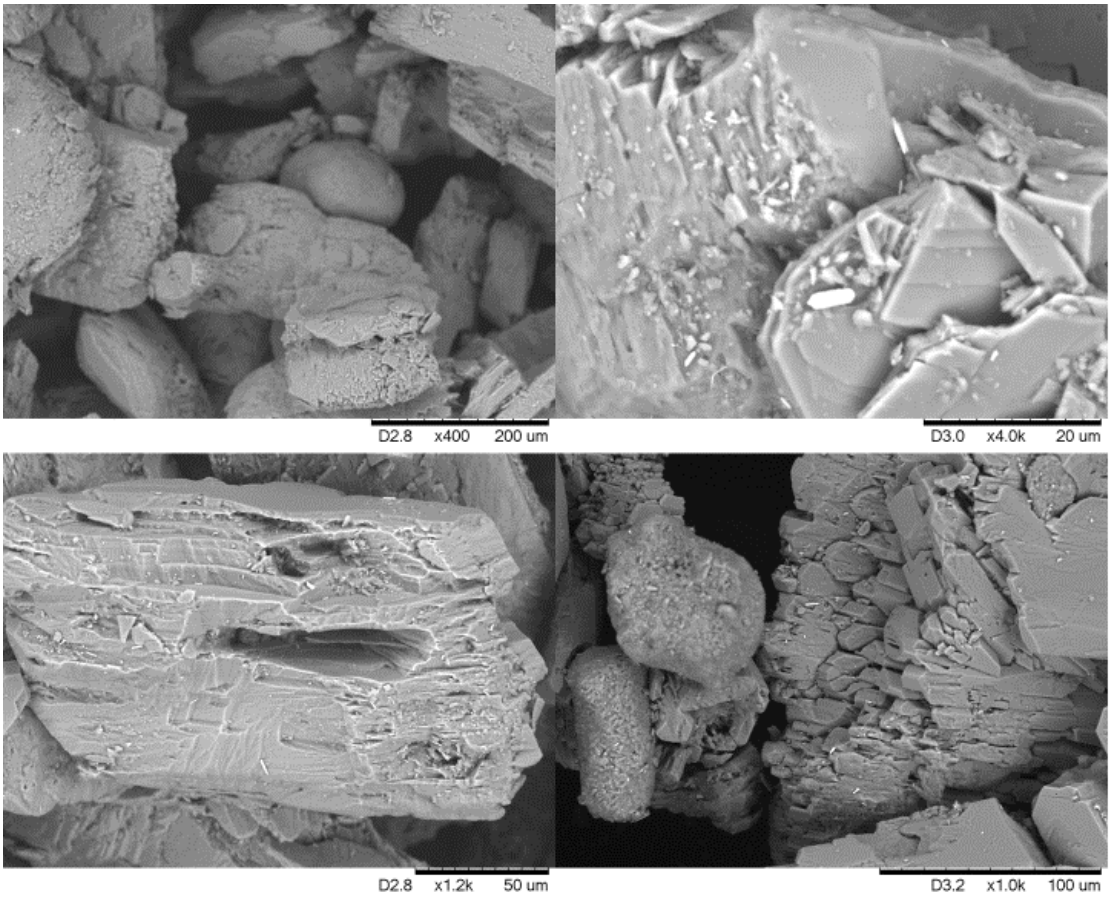

Figure 7b: Scanning electron micrographs of 12cm-deep sediment samples at Site Playa Lake. Compared to the surface crusts, these samples contained almost no acicular crystals.

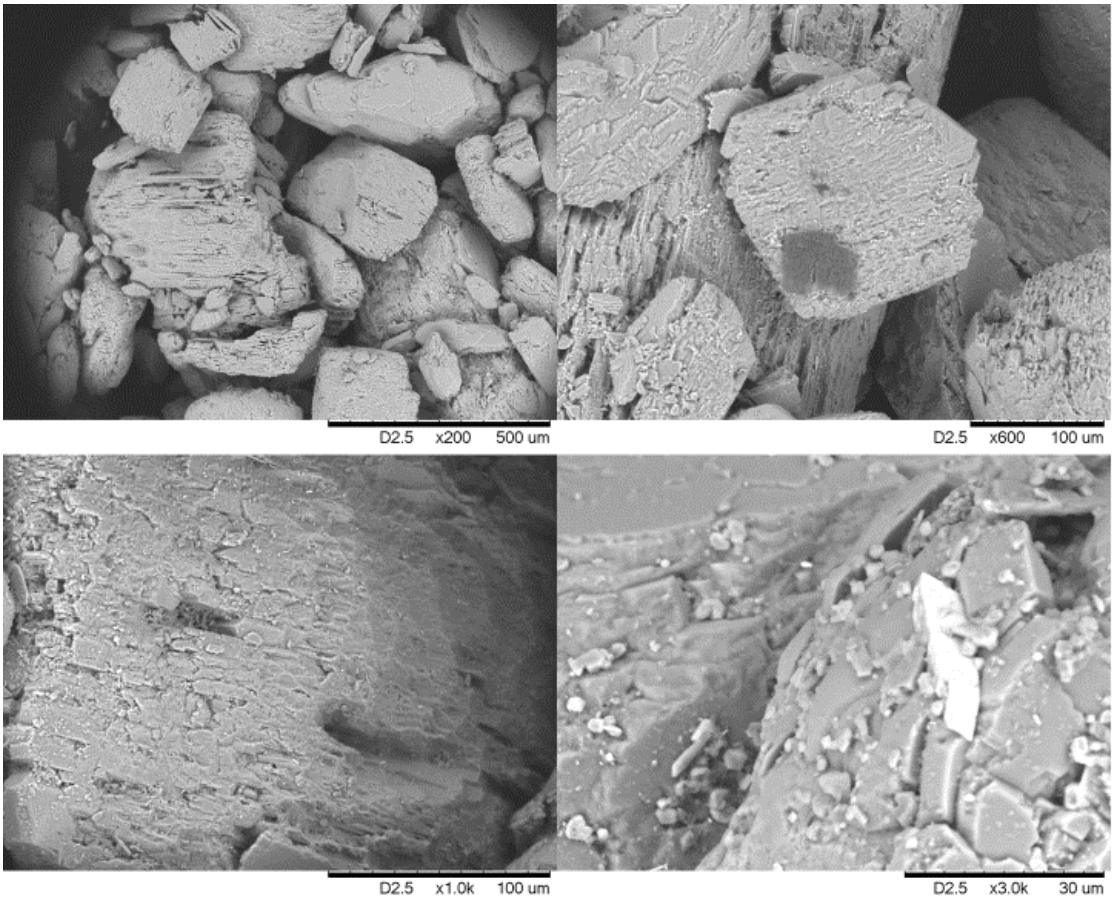

Figure 7c: Scanning electron micrographs of 32cm-deep sediment samples at Site Playa Lake. Phases of distinct morphology and electron density from the matrix grains become rare in these samples although a few dark patches were observed. The surfaces of the matrix gypsum grains become rougher, however.

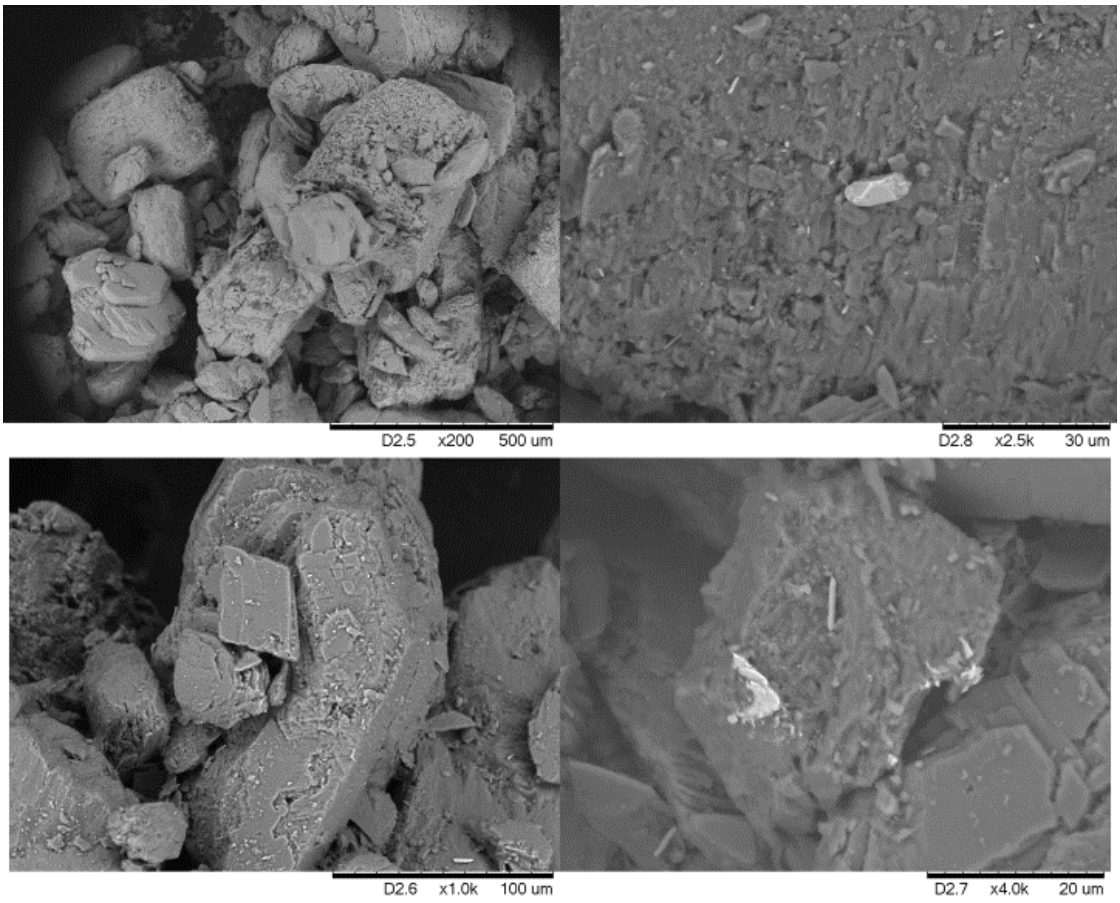

Figure 7d: Scanning electron micrographs of 42cm-deep sediment samples at Site Playa Lake. At this depth the presence of crystals and pitting is rare. Most grains show no characteristics of interest aside from coatings of a more electron dense substance (bottom right).

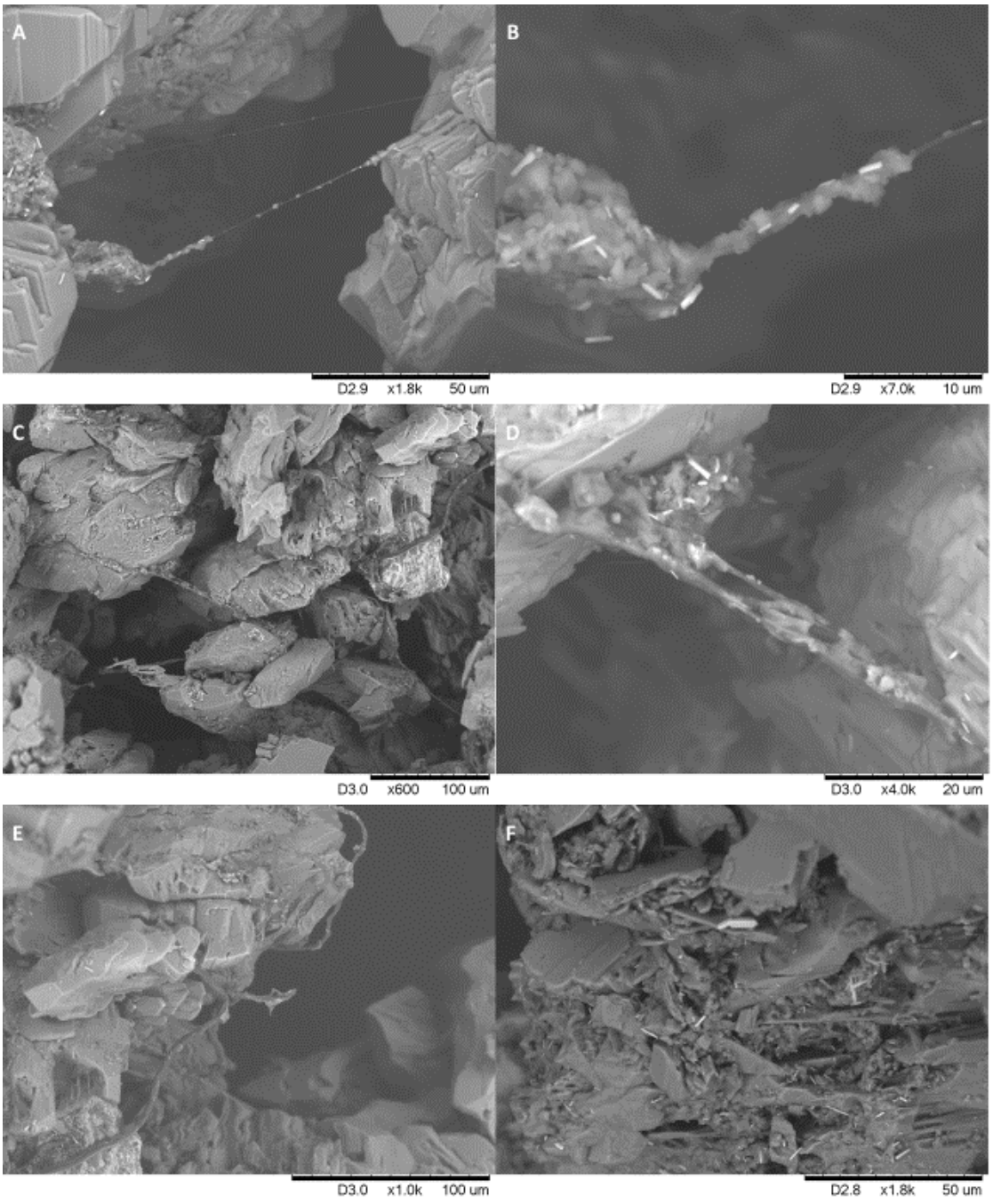

Figure 8: Scanning electron micrographs of crust sediment samples from Site Interdune. Slimy aggregates and structures indicative of biological activities are commonly present. Intensive surface pitting are also spotted. Crystals/particles of distinct morphology and crystal habits than the matrix grains were largely associated with the slimy aggregates.

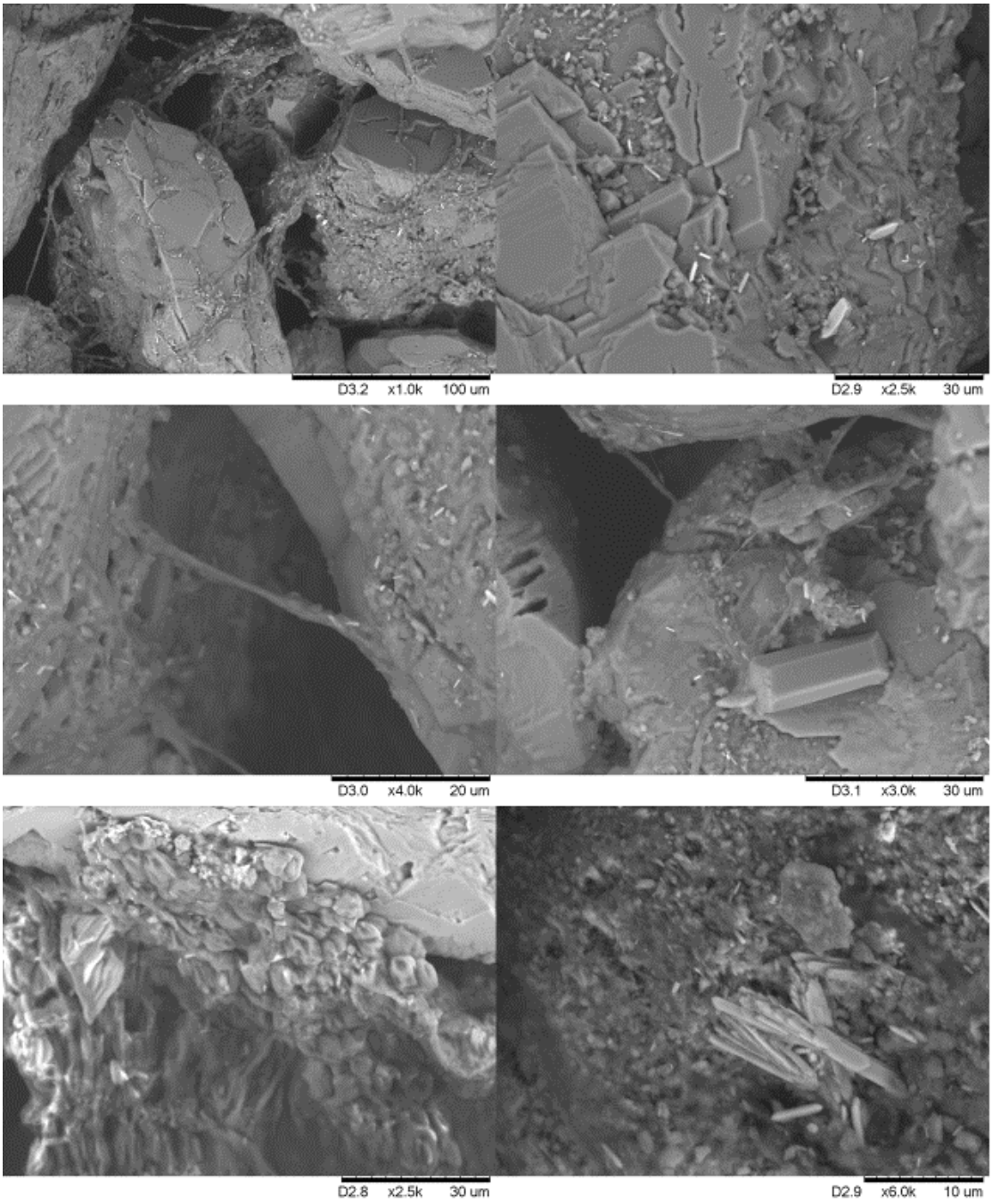

Figure 9: Scanning electron micrographs of crust sediment samples from Site Alkali Flat. Slimy aggregates and structures indicative of biological activities are found in these samples as well as several unique morphologies not seen in crust samples of other sites. Once again crystals of distinct morphology and crystal habits than the matrix grains were largely associated with the slimy aggregates.

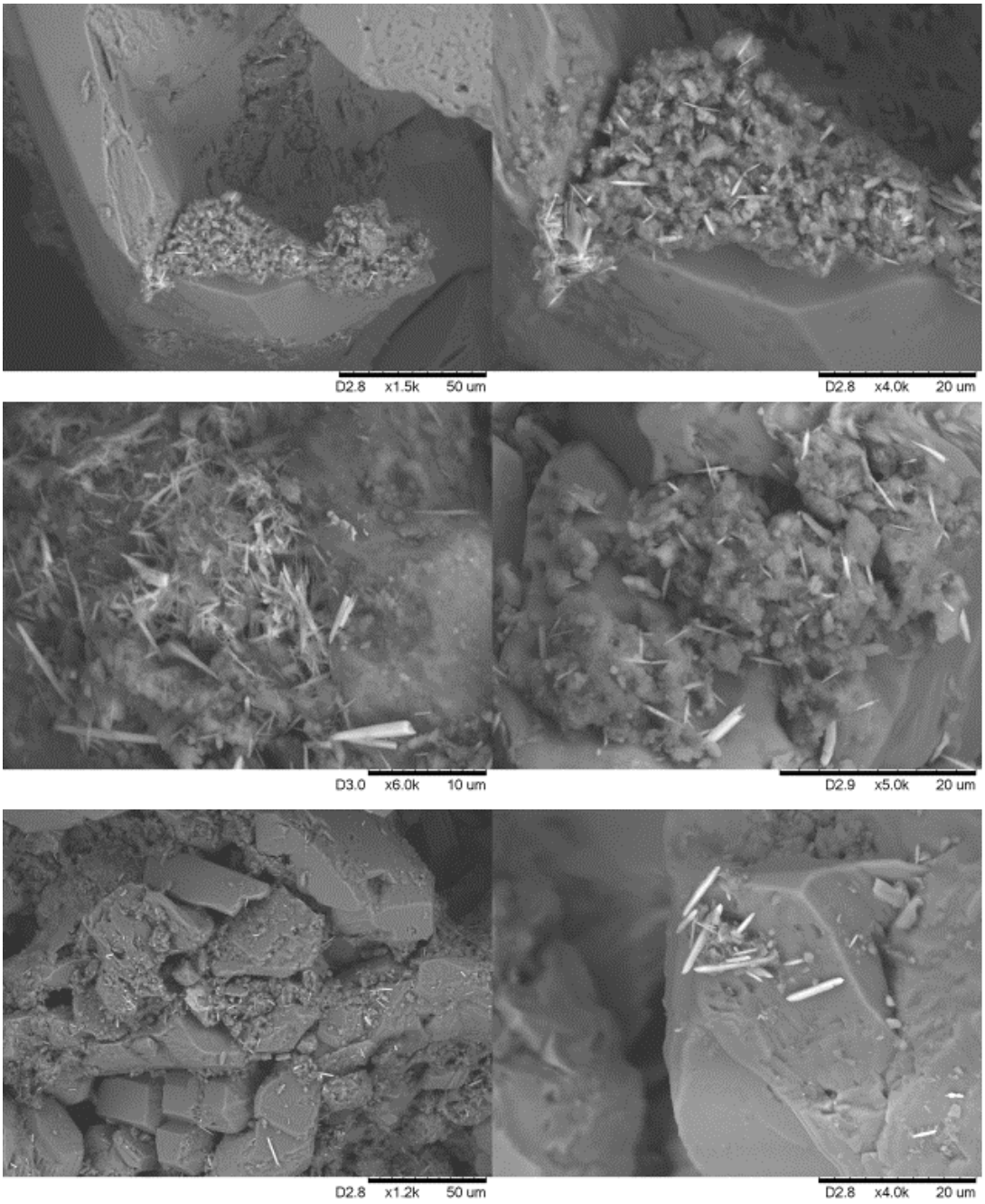

Figure 10: Scanning electron micrographs of crust sediment samples from Site Near Interdune Puddle. Slimy aggregates (i.e., biofilm-like structure) in this sample are covered in smaller needlelike crystals. The crystals appear to exist in higher amounts in proximity to the biofilm-like structures. Additionally, the biofilms seem to be infilling the pits within the sediment grains.

References

Anato, S. M., Hassan, I., Wang, J., Lee, P. L., & Toby, B. H. (2008). State-of-the-art high-resolution powder X-ray diffraction (HRPXRD) illustrated with rietveld structure refinement of quartz, sodalite, tremolite, and meionite. Canadian Mineralogist, 46(6), 1501–1509. https://doi.org/10.3749/canmin.46.6.1501

Araki, T., & Zoltai, T. (1967). Refinement of the crystal structure of a glauberite. American Mineralogist, 52, 1272–1277.

Barbieri, R., & Stivaletta, N. (2011). Continental evaporites and the search for evidence of life on Mars. Geological Journal, 46(6), 513–524. https://doi.org/10.1002/gj.1326

Baumgartner, L. K., Reid, R. P., Dupraz, C., Decho, A. W., Buckley, D. H., Spear, J. R., … Visscher, P. T. (2006). Sulfate reducing bacteria in microbial mats: Changing paradigms, new discoveries. Sedimentary Geology, 185(3-4 SPEC. ISS.), 131–145. https://doi.org/10.1016/j.sedgeo.2005.12.008

Benison, K. C., & Bowen, B. B. (2013). Extreme sulfur-cycling in acid brine lake environments of Western Australia. Chemical Geology, 351, 154–167. https://doi.org/10.1016/j.chemgeo.2013.05.018

Bezou C, Nonat A, Mutin J C, Christensen A N, L. M. S. (1995). Of the crystal structure of gamma-CaSO4, CaSO4*0.5(H2O), and CaSO4*0.6(H2O) by powder diffraction methods. Journal of Solid State Chemistry, (117), 165–176.

Bisson, K. M., Welch, K. A., Welch, S. A., Sheets, J. M., Lyons, W. B., Levy, J. S., & Fountain, A. G. (2015). Patterns and Processes of Salt Efflorescences in the McMurdo region, Antarctica. Arctic, Antarctic, and Alpine Research, 47(3), 407–425. https://doi.org/10.1657/aaar0014-024

Blair, T. C., Clark, J. S., & Wells, S. G. (1990). Quaternary continental stratigraphy, landscape evolution, and application to archeology: Jarilla piedmont and Tularosa graben floor, White Sands Missile Range, New Mexico. GSA Bulletin, 102(6), 749–759.

Buck, B. J., King, J., & Etyemezian, V. (2011). Effects of Salt Mineralogy on Dust Emissions, Salton Sea, California. Soil Science Society of America Journal, 75(5), 1971. https://doi.org/10.2136/sssaj2011.0049

Cook, J., Edwards, A., Takeuchi, N., & Irvine-Fynn, T. (2016). Cryoconite: The dark biological secret of the cryosphere. Progress in Physical Geography, 40(1), 66–111. https://doi.org/10.1177/0309133315616574

de Villiers, J. P. R. (1971). Crystal structures of aragonite, strontianite, and witherite. American Mineralogist, 56, 758–767.

Dong, H., Rech, J. A., Jiang, H., Sun, H., & Buck, B. J. (2007). Endolithnic cyanobacteria in soil gypsum: Occurences in Atacama (Chile), Mojave (United States), and Al-Jafr Basin (Jordan) Deserts. Journal of Geophysical Research: Biogeosciences, 112(2), 1–11. https://doi.org/10.1029/2006JG000385

Farias, M. E., Rasuk, M. C., Gallagher, K. L., Contreras, M., Kurth, D., Fernandez, A. B., … Visscher, P. T. (2017). Prokaryotic diversity and biogeochemical characteristics of benthic microbial ecosystems at La Brava, a hypersaline lake at Salar de Atacama, Chile. PLoS ONE, 12(11), 1–25. https://doi.org/10.1371/journal.pone.0186867

Fryberger, S. G. (2001). Geological Overview of White Sands National Monument. Retrieved from http://www.nature.nps.gov/geology/parks/whsa/geows/index.htm

Fryberger, S. G. (2003). Geology of White Sands National Monument. Retrieved from www2.nature.nps.gov/geology/parks/whsa/

Glamoclija, M., Fogel, M. L., Steele, A., & Kish, A. (2012). Microbial Nitrogen and Sulfur Cycles at the Gypsum Dunes of White Sands National Monument, New Mexico. Geomicrobiology Journal, 29(8), 733–751. https://doi.org/10.1080/01490451.2011.608111

Graf, D. L. (1961). Crystallographic tables for the rhombohedral carbonates. American Mineralogist, 46(11–12), 1283–1316.

Gumulya, Y., Boxall, N. J., Khaleque, H. N., Santala, V., Carlson, R. P., & Kaksonen, A. H. (2018). In a quest for engineering acidophiles for biomining applications: Challenges and opportunities. Genes, 9(2). https://doi.org/10.3390/genes9020116

Hughes, K. A., & Lawley, B. (2003). A novel Antarctic microbial endolithic community within gypsum crusts. Environmental Microbiology, 5(7), 555–565. https://doi.org/10.1046/j.1462-2920.2003.00439.x

Ikuma, K., Decho, A. W., & Lau, B. L. T. (2013). The Extracellular Bastions of Bacteria — A Biofilm Way of Life. Nature Education Knowledge, 4, 1–11.

Karnachuk, O., Kurochkina, S., & Tuovinen, O. (2002). Growth of sulfate-reducing bacteria with solid-phase electron acceptors. Applied Microbiology and Biotechnology, 58(4), 482–486. https://doi.org/10.1007/s00253-001-0914-3

Kocureka, G., Carra, M., Ewing, R., Havholm, K. G., Nagar, Y. C., & Singhvi, A. K. (2007). White Sands Dune Field, New Mexico: Age, dune dynamics and recent accumulations. Sedimentary Geology, 197(3–4), 313–331.

Kondo, R., Nedwell, D. B., Purdy, K. J., & Silvana, Q. S. (2004). Detection and Enumeration of Sulphate-Reducing Bacteria in Estuarine Sediments by Competitive PCR. Geomicrobiology Journal, 21(3), 145–157.

Langford, R. P. (2003). The Holocene history of the White Sands dune field and influences on eolian deflation and playa lakes. Quaternary International, 104(1), 31–39.

Langford, R. P., Rose, J. M., & White, D. E. (2009). Groundwater salinity as a control on development of eolian landscape: An example from the White Sands of New Mexico. Geomorphology, 105(1–2), 39–49. https://doi.org/10.1016/j.geomorph.2008.01.020

Lorenzo, D., & Valls, M. (2002). Exploiting the genetic and biochemical capacities of bacteria for the remediation of heavy metal pollution. FEMS Microbiology Reviews, 26(4), 327^338.

Mansor, M., Berti, D., Hochella, M. F., Murayama, M., & Xu, J. (2019). Phase, morphology, elemental composition, and formation mechanisms of biogenic and abiogenic Fe-Cu-sulfide nanoparticles: A comparative study on their occurrences under anoxic conditions. American Mineralogist, 104(5), 703–717. https://doi.org/10.2138/am-2019-6848

Marnocha, C. L., & Dixon, J. C. (2014). Endolithic bacterial communities in rock coatings from Kärkevagge, Swedish Lapland. FEMS Microbiology Ecology, 90(2), 533–542. https://doi.org/10.1111/1574-6941.12415

McKay, C. P., Rask, J. C., Detweiler, A. M., Bebout, B. M., Everroad, R. C., Lee, J. Z., … Al-Farraj, A. (2016). An Unusual Inverted Saline Microbial Mat Community in an Interdune Sabkha in the Rub' al Khali (the Empty Quarter), United Arab Emirates. PloS One, 11(3), e0150342. https://doi.org/10.1371/journal.pone.0150342

McKee, E. D. (1966). Structures Of Dunes At White Sands National Monument, New Mexico (And A Comparison With Structures Of Dunes From Other Selected Areas). Sedimentology, 7.

Muyzer, G., & Stams, A. J. M. (2008). The ecology and biotechnology of sulphate-reducing bacteria. Nature Reviews Microbiology, 6(6), 441–454. https://doi.org/10.1038/nrmicro1892

Natalicchio, M., Dela Pierre, F., Lugli, S., Lowenstein, T. K., Feiner, S. J., Ferrando, S., … Clari, P. (2014). Did late miocene (Messinian) gypsum precipitate from evaporated marine brines? Insights from the piedmont basin (Italy). Geology, 42(3), 179–182. https://doi.org/10.1130/G34986.1

Neculita, C.-M., Zagury, G. J., & Bussière, B. (2007). Passive Treatment of Acid Mine Drainage in Bioreactors using Sulfate-Reducing Bacteria. Journal of Environment Quality, 36(1), 1. https://doi.org/10.2134/jeq2006.0066

Newton, B. T., & Allen, B. (2014). Hydrologic Investigation at White Sands National Monument. New Mexico Bureau of Geology and Mineral Resources, Open-file.

NPS. (n.d.). Geology of White Sands.

Paolo Ballirano, Adriana Maras, Simone Meloni, R. C. (2001). The monoclinic I2 structure of bassanite, calcium sulphate hemihydrate. European Journal of Mineralogy, 13, 985–993.

Pizzi, J. (2018). Understanding How Microbes Survive Water-Restricted Environments from a Mineral Perspective: A Case Study Based in White Sands.

Poch, R. M., De Coster, W., & Stoops, G. (1998). Pore space characteristics as indicators of soil behaviour in gypsiferous soils. Geoderma, 87(1–2), 87–109.

Rabizadeh, T., Peacock, C. L., & Benning, L. G. (2014). Carboxylic acids: effective inhibitors for calcium sulfate precipitation? Mineralogical Magazine, 78(6), 1465–1472. https://doi.org/10.1180/minmag.2014.078.6.13

Ramierez, S. (2017). SHALLOW-SUBSURFACE MICROBIAL ECOLOGY AND SEDIMENT-GROUNDWATER INTERFACE IN SULFATE-RICH PLAYA AT WHITE SANDS NATIONAL MONUMENT, NEW MEXICO By.

Ramsdell, L. S. (1925). The crystal structures of some metallic sulfides. American Mineralogist, 10, 281–304.

Rettig, S. J., & Trotter, J. (1987). Refinement of the structure of orthorhombic sulfur. Acta Crystallographica, C43, 2260–2262.

Schofield, P. F., Knight, K. S., & Stretton, I. C. (1996). Thermal expansion of gypsum investigated by neutron powder diffraction. American Mineralogist, 81, 847–851.

Shahid, S. A., Abdelfattah, M. A., & Wilson, M. A. (2015). A Unique Anhydrite Soil in the Coastal Sabkha of Abu Dhabi Emirate. Soil Horizons, 48(4), 75. https://doi.org/10.2136/sh2007.4.0075

Shen, Y., & Buick, R. (2004). The antiquity of microbial sulfate reduction. Earth-Science Reviews, 64(3–4), 243–272. https://doi.org/10.1016/S0012-8252(03)00054-0

Shen, Y., Buick, R., & Canfield, D. E. (2001). Isotopic evidence for microbial sulphate reduction in the early Archaean era. Nature, 410(6824), 77–81. https://doi.org/10.1038/35065071

Steinfink, H., & Sans, F. J. (1959). Refinement of the crystal structure of dolomite. American Mineralogist, 44(5–6), 679–682.

Stivaletta, N., Barbieri, R., & Billi, D. (2012). Microbial Colonization of the Salt Deposits in the Driest Place of the Atacama Desert (Chile). Origins of Life and Evolution of Biospheres, 42(2), 187–200. https://doi.org/10.1007/s11084-012-9289-y

Takai, K., Nunoura, T., Ishibashi, J. I., Lupton, J., Suzuki, R., Hamasaki, H., … Horikoshi, K. (2008). Variability in the microbial communities and hydrothermal fluid chemistry

at the newly discovered Mariner hydrothermal field, southern Lau Basin. Journal of Geophysical Research: Biogeosciences, 113(2). https://doi.org/10.1029/2007JG000636

Tang, K., Baskaran, V., & Nemati, M. (2009). Bacteria of the sulphur cycle: An overview of microbiology, biokinetics and their role in petroleum and mining industries. Biochemical Engineering Journal, 44(1), 73–94. https://doi.org/10.1016/j.bej.2008.12.011

Visscher, P. T., Prins, R. A., & van Gemerden, H. (1992). Rates of sulfate reduction and thiosulfate consumption in a marine microbial mat. FEMS Microbiology Ecolog, 86, 283–294.

Walker, D., Verma, P. K., Cranswick, L. M. D., Jones, R. L., Clark, S. M., & Buhre, S. (2004). Halite-sylvite thermoelasticity. American Mineralogist, 89, 204–210.

Westrich, J. T., & Berner, R. A. (1984). The role of sedimentary organic matter in bacterial sulfate reduction: The G model tested. Limnology and Oceanography, 29(2), 236–249. https://doi.org/10.4319/lo.1984.29.2.0236

Wierzchos, J., DiRuggiero, J., Vítek, P., Artieda, O., Souza-Egipsy, V., Škaloud, P., … Ascaso, C. (2015). Adaptation strategies of endolithic chlorophototrophs to survive the hyperarid and extreme solar radiation environment of the Atacama Desert. Frontiers in Microbiology, 6(SEP), 1–17. https://doi.org/10.3389/fmicb.2015.00934

Worman, F. S., Kurota, A., & Hogan, P. (2019). Dunefield geoarchaeology at White Sands National Monument, New Mexico, USA: Site formation, resource use, and dunefield dynamics. Geoarchaeology, 34(1), 42–61.

Zentilli, M., Omelon, C. R., Hanley, J., & LeFort, D. (2019). Paleo-Hydrothermal Predecessor to Perennial Spring Activity in Thick Permafrost in the Canadian High Arctic, and Its Relation to Deep Salt Structures: Expedition Fiord, Axel Heiberg Island, Nunavut. Geofluids, 2019, 1–33. https://doi.org/10.1155/2019/9502904

Vita

Brandon N LaJoie successfully defended his thesis and graduated with a M.S. in Geology in the summer of 2019. His hunger for discovery and his skills as a scientist were honed through the course of his Bachelor's Degree in Geology and chemistry minor at LSSU. Brandon worked at the NanoGeoBio Lab under the guidance of Dr. Jie Xu, where he studied the relation between sulfur reducing bacterial populations and their effect on hydrous sulfate sediments. Brandon took part in an internship with the Eastern Upper Peninsula Regional Planning and Development office and participated in the International Barrel Award competition of AAPG in 2018. Brandon hopes his project will inspire further research for the scientific community as a whole into the questions that still surround biocrusts. He seeks to use the knowledge he has gathered during his education to work for an environmental agency.

Contact Information (optional) : blajoie@miners.utep.edu

This thesis was typed by Brandon N LaJoie